

1 **Integrated cell type-specific analysis of blood and gut identifies matching eQTL for 140 IBD**
2 **risk loci and entrectinib as possible repurposing candidate.** [132 characters]

3

4 *Hélène Perée¹, Viacheslav A Petrov^{1§}, Yumie Tokunaga^{1§}, Alexander Kvasz¹, Sophie Vieujean²,*
5 *Sarah Regimont¹, Myriam Mni¹, Marie Wéry¹, Samira Azarzar², Sophie Jacques¹, Nicolas*
6 *Fouillien¹, Latifa Karim³, Manon Deckers³, Emilie Detry³, Alice Mayer⁴, Raafat Stephan⁵, Keith*
7 *Harshman⁶, Yasutaka Mizoro¹, Catherine Reenaers², Catherine Van Kemseke², Odile Warling²,*
8 *Virginie Labille², Sophie Kropp², Maxime Poncin², Anne Catherine Moreau², Benoit Servais²,*
9 *Jean-Philippe Joly², SYSCID Consortium, BRIDGE Consortium, Wouter Coppieters³, Emmanouil*
10 *Dermitzakis⁶, Edouard Louis², Michel Georges^{1,7#}, Haruko Takeda¹, Souad Rahmouni^{1#}.*

11

12 1. Unit of Animal Genomics, GIGA Institute & Faculty of Veterinary Medicine, University of
13 Liège, Belgium. 2. Department of Gastroenterology, Faculty of Medicine, CHU & GIGA
14 Institute, University of Liège, Belgium. 3. Genomics core facility, GIGA Institute, University of
15 Liège, Belgium. 4. GIGA bioinformatics core facility, GIGA Institute, University of Liège,
16 Belgium. 5. GIGA in vitro imaging and cell sorting core facility, GIGA Institute, University of
17 Liège, Belgium. 6. Genomics core facility, University of Geneva, Switzerland. 7. Welbio
18 Research Institute, Belgium.

19

20 § Contributed equally. # Co-senior and corresponding authors: srahmouni@uliege.be,
21 michel.georges@uliege.be.

22

23

1 **Abstract** [129 words]

2 Genes whose expression is affected in a consistent manner by GWAS-identified risk variants
3 and the disease process, constitute preferred drug targets. We herein combine integrated cis-
4 eQTL analysis in 27 blood cell populations and 43 intestinal cell types of the ileum, colon and
5 rectum, and information on gene expression in patients, to search for putative drug targets
6 for inflammatory bowel disease (IBD). We detect >95K cis-eQTL that affect >13K e-genes and
7 cluster in >24K regulatory modules (RM). We uncover matching RM for 140 risk loci,
8 implicating >300 e-genes not previously connected to IBD, and find 152 IBD-matching e-genes
9 whose expression is perturbed in the blood or gut of patients. We identify entrectinib, a small
10 molecule inhibiting the NLRP3 inflammasome by binding NEK7, as a promising repurposing
11 candidate for IBD.

1 Introduction

2 The growing prevalence of common complex diseases (CCD) threatens the sustainability of
3 health care systems world-wide. There is a need for more effective prevention and treatment
4 [Busse *et al.*, 2010; Schumacher *et al.*, 2016; Jakab *et al.*, 2018].

5 Predisposition to most CCD has a considerable inherited component [Polubriaginoff *et al.*,
6 2018]. Accordingly, GWAS with case-control cohorts in the tens to hundreds of thousands of
7 individuals have nearly systematically uncovered tens to hundreds of risk loci that explain up
8 to ~50% of the heritability [Visscher *et al.*, 2017; Abdelloui *et al.*, 2023]. Identifying the genes
9 that are perturbed by the risk variants in these loci is considered a key goal, as these
10 constitute preferred drug targets for the pharmaceutical industry [King *et al.*, 2019; Burgess
11 *et al.*, 2023; Trajonaska *et al.*, 2023; Minikel *et al.*, 2024].

12 A common feature of CCD is that the majority of associations are driven by regulatory variants
13 as opposed to coding variants. For example, amongst the more than 200 risk loci now mapped
14 for inflammatory bowel disease (IBD), only 14 encompass ORF-altering variants in the
15 corresponding credible sets (i.e., the set of variants in high linkage disequilibrium (LD) that
16 have a high posterior probability to be causal), thereby rather convincingly pinpointing
17 causative genes and hence putative drug targets [Sazonovs *et al.*, 2023]. The prevailing
18 hypothesis is that for the remaining loci, regulatory variants perturb the expression of
19 causative genes in *cis*. The challenges are to identify the causative regulatory variants in the
20 credible sets, and – most importantly - the genes they perturb in *cis*. A common approach to
21 achieve the latter is by means of eQTL analyses performed in disease relevant cell types
22 collected from healthy individuals. Indeed, it is reasonable to assume that: (i) the effect of
23 most regulatory variants will manifest by genotype-specific differences in steady state
24 messenger levels (i.e., eQTL effects), and (ii) the corresponding eQTL effects, caused by mostly
25 common variants, are detectable in healthy individuals as well. If a *cis*-eQTL underpins a
26 GWAS-identified risk locus it will exhibit an association pattern (the vector of association
27 $\log(1/p)$ values of all the SNPs in the locus with the gene's expression levels, henceforth
28 referred to as EAP for expression association pattern) that is very similar to the association
29 pattern of the risk locus (henceforth referred to as DAP for disease association pattern),
30 provided that the GWAS and eQTL studies were conducted in cohorts of same ethnicity (and
31 hence same LD structure). A number of colocalization methods have been developed to

1 quantify the resemblance between DAP and EAP [f.i. Giambartolomei *et al.*, 2014; Zhu *et al.*,
2 2016; Hormozdiari *et al.*, 2016; Momozawa *et al.*, 2018].

3 Several eQTL datasets have been assembled towards that goal, admittedly still heavily biased
4 in favor of Northern European ancestry. The most prominent of those is the GTEx cohort that
5 provides eQTL information for 52 tissues in up to 838 subjects [GTEx Consortium, 2020]. A
6 common observation from such colocalization experiments is that “matching” eQTL are only
7 found for ~25% of risk loci, raising questions about the molecular underpinnings of the still
8 majority of risk loci [Umans *et al.*, 2021]. For example, we previously identified matching
9 eQTL in 63 of 200 analyzed IBD risk loci using a catalog of 23,650 eQTL identified using
10 transcriptome data of six circulating immune cell types and intestinal biopsies at three
11 locations (CEDAR-1 dataset) [Momozawa *et al.*, 2018].

12 A plausible explanation of this still high proportion of “orphan” risk loci, is that the
13 corresponding eQTL remain to be discovered. This could be because the relevant cell
14 populations were underrepresented in the (often heterogeneous) samples studied to date,
15 because the manifestation of the eQTL is context dependent (f.i. after initiation of the disease
16 process), or because the eQTL discovered thus far (with small sample sizes when compared
17 to disease GWAS) are distinct from the ones that drive CCD [Mostafavi *et al.*, 2023].

18 In this work, we followed up on the first hypothesis, i.e., the relevant cell populations are
19 underrepresented in the samples studied to date, in the context of IBD. Towards that goal
20 we established the CEDAR-2 eQTL dataset based on (i) bulk transcriptome data from 27
21 circulating immune cell populations for 200 healthy individuals, and (ii) single-cell RNA
22 (scRNA) transcriptome data for intestinal biopsies collected at three locations (terminal ileum,
23 transverse colon and rectum) from 60 healthy individuals. Using this dataset, we herein report
24 the identification of matching *cis*-eQTL for 140 of 206 examined IBD risk loci, identify more
25 than 300 novel candidate causal genes, and pinpoint opportunities for drug repurposing.

26

27 Results

28 ***60,113 cis-eQTL affecting 11,874 eQTL genes in 27 circulating immune cell populations***
29 ***cluster in 22,067 cis-acting regulatory modules.***

1 We collected peripheral blood from 251 healthy individuals of both sexes (STable 1). We
2 genotyped all individuals with Illumina's OmniExpress array interrogating ~700K SNPs, and
3 augmented genotype data to ~6.3 million (M) variants by imputation. For each individual, in
4 addition to collecting peripheral blood mononuclear cells (PBMC), we sorted 26 distinct
5 immune cell populations from whole blood by fluorescent activated or magnetic cell sorting
6 (FACS or MACS) (SFig. 1; STable 2). We produced next generation sequencing (NGS) libraries
7 for each of the 27 cellular fractions of each individual (5,292 mRNA SMART-Seq HT libraries in
8 total), and generated an average of ~12.6M, 2 x 150 bp (3,180 libraries) or ~13M, 2 x 50 bp
9 (2,112 libraries) paired-end reads per library on Illumina instruments (STable 3).
10 Transcriptome data were used to check the assignment of libraries to individuals and cell
11 types, and errors corrected (SFig. 2A-B). The numbers of genes detected averaged 16,615 per
12 cell type (range: 12,776 – 19,042) (STable 4). Hierarchical clustering of cell types based on
13 average gene expression levels generated a dendrogram largely consistent with
14 hematopoietic ontogeny (SFig. 2C).

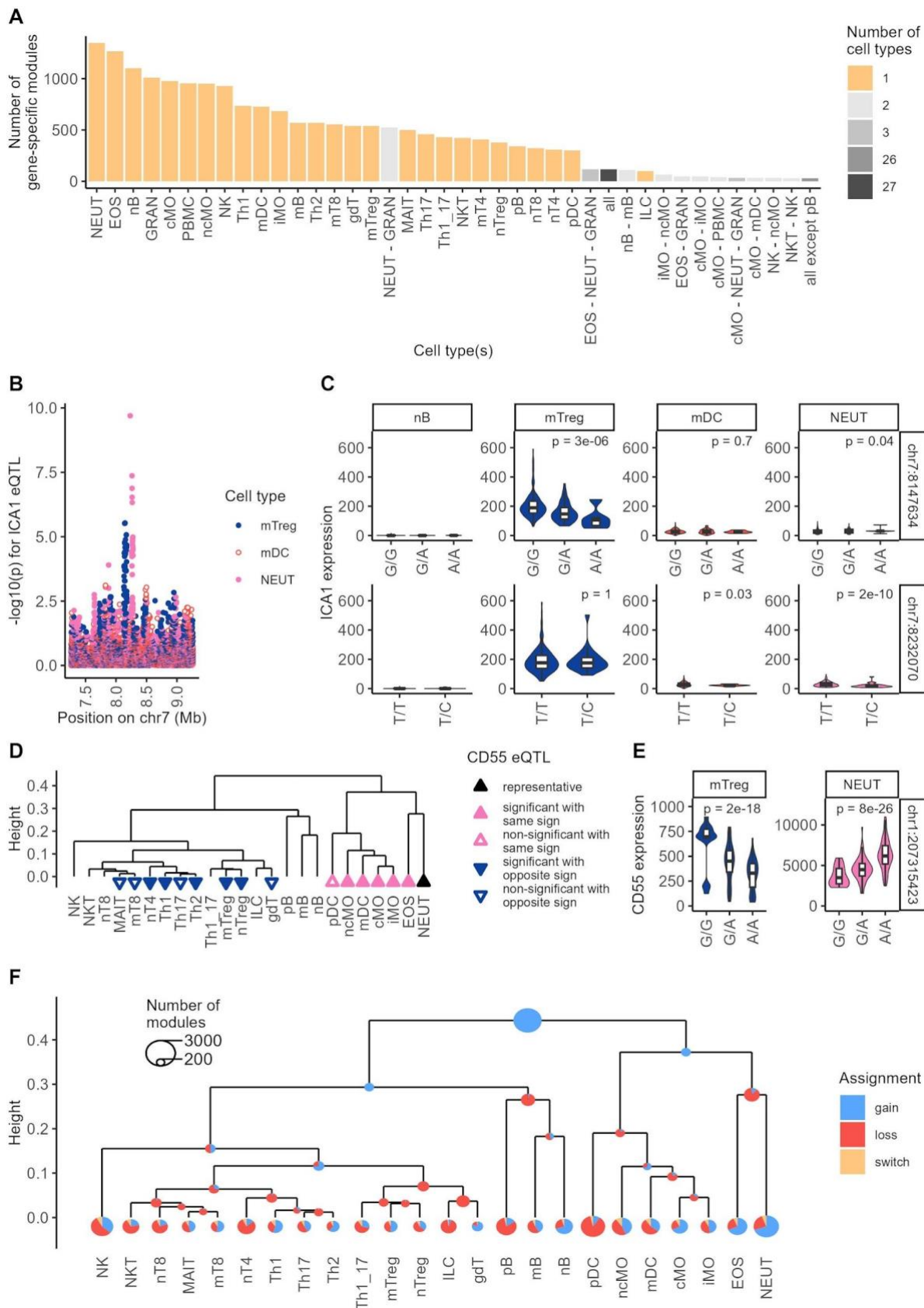
15 We performed *cis*-eQTL analyses using a custom-made pipeline including QTLtools [Delaneau
16 *et al.*, 2017], regressing gene expression level on alternate allele dosage and including an
17 average of 24.4 expression principal components (PC) (range: 13 - 36) in the model (STable 4;
18 M&M). We identified 60,113 eQTL (within cell type FDR \leq 0.05), influencing the expression
19 of 11,874 eQTL genes (e-genes) (STable 5). The number of eQTL detected per cell type
20 (average: 2,226; range: 608 – 3,448) was largely determined by the number of samples
21 available for analysis ($r^2=0.67$) (SFig. 3A). The number of eQTL detected in PBMC was larger
22 than expected given sample numbers, consistent with PBMC encompassing multiple cell
23 types. The number of eQTL detected in plasmocytes was lower than expected given sample
24 numbers. Controlling for the variable abundance of immunoglobulin transcripts did not
25 increase the number of detected plasmocyte eQTL (SFig. 3B). On average, *cis*-eQTL explained
26 19.7% (range: 3.2% - 83.6%) of variance in gene expression level (SFig. 3C). Significant
27 secondary *cis* signals (range: 2 - 5) were detected for 6% of *cis*-eQTL, when repeating the eQTL
28 analysis conditional on the previous signals (SFig. 3D).

29 eQTL affecting the same gene in multiple cell types were merged if sharing a similar
30 association pattern (EAP) as evaluated using theta ($|\theta| \geq 0.6$) [Momozawa *et al.*, 2018],
31 yielding 23,831 distinct gene-specific modules (STable 6). Modules were augmented with
32 5,840 tier-2 eQTL that would nevertheless match ($|\theta| \geq 0.6$) at least one significant eQTL in

1 the module (see M&M). Modules can be characterized by a vector of 0 and 1 that indicates
2 in which cell type(s) the module is active. The 31 most common vectors were dominated by
3 17,439 modules (i.e., 73.2%) that are active in only one of each of the 27 cell types, and
4 included 117 modules that are – *a contrario* - active in all 27 cell types (Fig. 1A). The
5 overdispersion of the number of active cell types (i.e., excess of modules active either in very
6 few or many cell types) was highly significant ($p < 0.001$) (see M&M). Sharing of modules by
7 cell types was largely determined by their ontogenic proximity (SFig. 3E).

8 A module can be active in cell type A but not in cell type B because: (i) the gene is expressed
9 in cell type A but not in cell type B, (ii) the gene is expressed in both cell types but the eQTL is
10 only active in cell type A, or (iii) the gene is in distinct modules in cell type A and B (i.e.,
11 different EAP in cell types A and B). Expression of the gene was below detection levels in cell
12 type B (i.e., first scenario) in 17.7% of cases. Analysis of the modules indicated that the third
13 scenario (module switch) accounts for 8.5% of cases. We devised an interaction test to
14 evaluate the importance of scenario 2 (see M&M) in the remaining 73.8% of the cases. We
15 estimated the proportion of alternative hypothesis (π_1) following Storey *et al.* [2003] at
16 97.3%, hence supporting the fact that the eQTL was indeed not active in cell type B in 71.8%
17 of cases despite the fact that the gene was expressed in cell type B (Fig. 1B-C; SFig. 3F). For
18 modules active in more than one cell type, the direction of the effects was the same across
19 cell types in 96.1% of the cases, yet there were 250 cases for which the sign of the effect
20 switched between cell types (Fig. 1D-E; STable 6). The proportion of shared eQTL yet with
21 opposite sign increased with ontogenic distance between considered cell types as expected
22 ($p_{logit} = 4 \times 10^{-33}$; STable 7). Modules were assigned to nodes and leaves in the ontogenic
23 dendrogram using the patterns of module sharing across cell types (vectors of 0's and 1's)
24 (see M&M), suggesting extensive remodeling of eQTL activity during hematopoiesis, including
25 the presumed common loss of progenitor cell eQTL and gain of new eQTL by differentiated
26 cells, primarily involving different sets of genes (as the proportion of module switches was
27 limited) (Fig. 1F). Genes with *cis*-eQTL assigned towards the root (presumed to be active in
28 progenitor cells, $n=2,776$) were enriched in GO terms: antigen processing and presentation,
29 amino-acid metabolism, organic acid and small molecule metabolic processes, and cell
30 motility, while genes with *cis*-eQTL assigned towards the leaves ($n=9,201$) did not show
31 enrichment in any GO terms (STable 8).

1 We then merged gene-specific modules with matching EAP “across genes”, yielding a total of
2 22,067 *cis*-acting regulatory modules. Modules were augmented with 7,402 tier-2 eQTL
3 matching at least one significant *cis*-eQTL in the module, recruiting 759 extra genes (M&M;
4 STable 9). We observed 2,470 modules (11.2%) comprising more than one gene. On average
5 such multigenic modules encompassed 2.9 genes (range: 2 - 32) and were active in 9.3 cell
6 types (SFig. 3G). Gene-specific modules active in multiple (but not all) cell types had more
7 chance to join a multigenic module than gene-specific modules active in only one cell type
8 (SFig. 3H). eQTL effects with opposite sign (negative θ) were observed for 48.8% of multigenic
9 modules. For the 5,856 modules encompassing more than one EAP (whether from the same
10 or different genes), we combined the constituent association patterns in a consensus EAP
11 representing the module (see M&M). We developed a web browser to visualize the activity
12 of the regulatory modules across the genome and cell types (SFig.
13 4; <https://tools.giga.uliege.be/cedar/publihpg>).



1
2 **Figure 1: (A)** Gene-specific modules grouped by cell type combinations in which they are active, and ordered
3 according to the frequency of occurrence (40 most frequent combinations out of 3,572 observed). The most
4 common modules are dominated cell type-specific ones, i.e., only active in one cell type (27 yellow bars). Also,
5 amongst the top 40 combinations, are those corresponding to modules that are active in all (i.e., ubiquitous

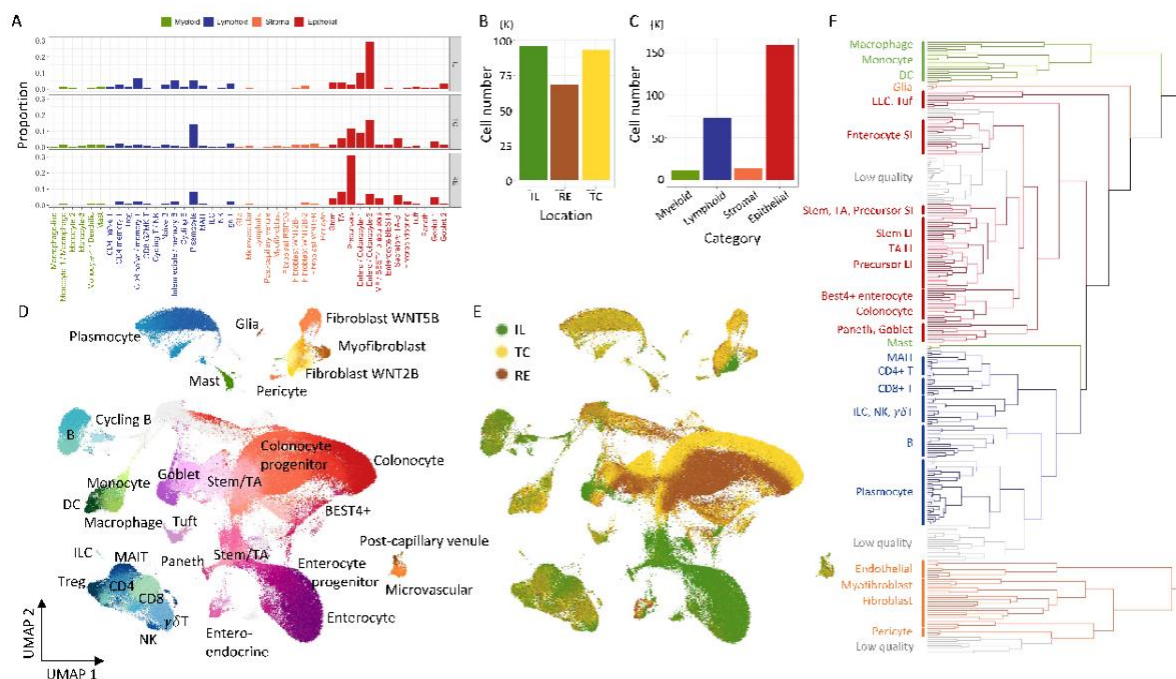
1 eQTL; black bar). The remaining combinations that are shown correspond to modules that are active in 2 or 3
2 closely related cell types (hence still very cell type-specific). Cell type abbreviations are as in STable 2. **(B-C)**
3 Example of a gene (*ICA1*) that is controlled by two distinct modules operating respectively in memory regulatory
4 T cells (mTreg, module #12,606, blue in EAP and violin plots) and neutrophils (NEUT, module #16,344, pink in
5 EAP and violin plots). Neither of these is active in myeloid dendritic cells (mDC, orange EAP and violin plot)
6 despite the fact that the gene is expressed at relatively high levels in this cell type (scenario 2). The gene is
7 expressed at very low levels in naïve B cells (nB) in which consequently neither module is active either (scenario
8 1). Individuals are sorted by genotype at the lead SNPs for modules #12,605 (upper row) and #16,344 (lower
9 row). **(D-E)** Example of a gene-specific eQTL module (*CD55*, module #678) that is active in 16 of the 24 shown
10 cell types, including all myeloid cell types, and nine of 12 types of T-cells (filled triangles: significant eQTL; empty
11 triangles (tier-2): non-significant eQTL but matching ($|\theta| \geq 0.6$) at least one of the significant eQTL in the
12 module). However, the sign of the eQTL (effect of the alternate allele) is opposite in myeloid cells (pink, upward
13 pointing triangles) and T lymphocytes (blue, downward pointing triangles). The reference sign is determined by
14 the most significant, “representative” eQTL in the module (black triangle). Violin plots show the distribution of
15 *CD55* expression (DESeq2 normalized expressions) in memory regulatory T cells (left, blue) and neutrophils
16 (right, pink) for individuals sorted by genotype at the lead variant for the consensus EAP. **(F)** Gains of gene-
17 specific modules were assigned to the “most recent common ancestor” (MRCA) node of all nodes/leaves in
18 which the module is active (blue segments). Losses of gene-specific modules were assigned to the MRCA node
19 of all descendent (of a node to which a module was assigned) nodes/leaves in which the module was not active
20 (red segments). If the loss of a module coincided with the gain of a module for the same gene, we assumed that
21 a module switch occurred (yellow segments). The diameter of the circles is indicative of the corresponding
22 numbers, *per* legend.

23

24 ***Single-cell RNA Seq analysis of intestinal biopsies reveals 35,010 eQTL affecting 3,007 genes*** 25 ***and clustering in 3,337 modules.***

26 We collected biopsies in the terminal ileum (IL), transverse colon (TC), and rectum (RE)
27 (locations) of 60 healthy individuals. Epithelium and lamina propria (fractions) were
28 separated, location- and fraction-specific cell suspensions hash-tagged, and subjected to
29 scRNA-Seq using a 10X Chromium platform and Illumina sequencers. We obtained quality-
30 filtered sequence data for a total of 293,801 cells from 57 individuals (5,154 cells per
31 individual on average). The number of reads per cell averaged 48,628, the number of unique
32 molecular identifiers (UMI) per cell 7,422, and the number of genes detected per cell 2,035
33 (STable 10). Cells were assigned to one of nine sets corresponding to anatomical location (IL,
34 TC, RE) and cell category (epithelial, immune, stromal) (see M&M). K-means clustering of the
35 cells, by set, yielded a total of 276 clusters. Samples were merged using Harmony [Korsunsky
36 *et al.*, 2019], and a hierarchical tree (of clusters) constructed using the Euclidean distances
37 between the clusters’ centroids in Harmony space. Leaves (corresponding to clusters in the
38 original nine cell sets) and nodes in the tree were assigned to 13 epithelial, 14 lymphoid, 6
39 myeloid and 10 stromal cell types (43 cell-types in total) using cell-type specific gene
40 signatures from the literature [Smillie *et al.*, 2019; Franzen *et al.*, 2019; Hao *et al.*, 2021;
41 Burclaff *et al.*, 2022; Ishikawa *et al.*, 2022; Hickey *et al.*, 2023; Kong *et al.*, 2023; Krzak *et al.*,

1 2023] (Fig. 2; SFig. 5&6; STable 11). Numbers of cells were relatively evenly distributed across
 2 the three anatomical locations (Fig. 2B). Epithelial cells were more abundant than lymphoid,
 3 myeloid and stromal fractions combined (Fig. 2C). Strikingly, myeloid, lymphoid and
 4 endothelial cells from the three locations overlapped well in UMAP space, while absorptive
 5 and secretory epithelial cells as well as fibroblast from distinct locations did not, supporting
 6 larger effects of location on the transcriptome for the latter (Fig. 2E). Paneth cells were
 7 exclusively observed in ileal samples as expected, while most other cell types were present in
 8 the three locations.
 9 Epithelial, stromal, myeloid and lymphoid cell types clustered in the tree as expected (except
 10 for glia and mast cells) (Fig. 2F). The segregation of ileal, colonic and rectal clusters occurred
 11 mostly at terminal branches of the tree, with the exception of absorptive epithelium, in
 12 agreement with the overlap in UMAP space (SFig. 6J).



13
 14 **Figure 2: (A)** Proportion of cells from ileal (IL), colonic (TC), and rectal (RE) biopsies assigned to 6 myeloid cell
 15 types (green), 14 lymphoid cell types (blue), 10 stromal cell types (orange) and 13 epithelial cell types (red). **(B)**
 16 Number of recovered quality-controlled (QC-ed) cells by anatomical location. **(C)** Number of recovered QC-ed
 17 cells by cell category. Colors are as in A. **(D)** UMAP of 293,801 QC-ed cells labeled by cell category (myeloid,
 18 lymphoid, stromal, epithelial) and cell-type within category. **(E)** Same UMAP as in D, labeled by anatomical
 19 location (colors as in B). **(F)** Hierarchical tree of 276 cell clusters (with 275 nodes). Four cell categories (myeloid,
 20 lymphoid, stromal, epithelial) are color-coded as in A and C. The main cell types within categories are labeled.
 21

22 We then conducted eQTL analyses separately by leaf and node across the tree (551 analyses
 23 in total). eQTL analyses were performed using the same custom-made pipeline including

1 QTLtools, using a pseudo-bulk approach and leaf/node-specific PEER factors [Stegle *et al.*,
2 2010] to correct for hidden confounders (including variable cell-type proportions) (SFig. 5).
3 We detected a total of 35,010 *cis*-eQTL (within leaf/node FDR ≤ 0.05) affecting 3,007 e-genes
4 (STable 12). The number of eQTL detected per leaf/node was largely determined by the
5 number of cells in the leaf/node with, however, a higher yield per cell for epithelial than for
6 the other cell categories. It plateaued at $\sim 1,100$ presumably limited by sample size (57
7 individuals) (Fig. 3A). A second independent effect was detected for 259 *cis*-eQTL, and a third
8 for two (STable 12). As for the circulating immune populations, we merged *cis*-eQTL affecting
9 the same gene in 3,345 gene-specific modules when sharing similar EAP ($|\theta| \geq 0.6$), and
10 augmented modules with 22,904 tier-2 eQTL that would nevertheless match at least one
11 significant eQTL in the module (see M&M) (STable 13). We assigned modules to the most
12 recent common ancestor (MRCA) of all active nodes/leaves. Modules mapping near the tree's
13 root were allocated to pairs of cell categories when possible. Most of the modules mapped
14 towards the root of the tree, as expected as this is where the number of cells per node is
15 largest and hence detection power is highest (Fig. 3B). However, the numbers of
16 leaves/nodes in which a module was active was over-dispersed: modules tended to be either
17 active in fewer leaves/nodes or in more leaves/nodes than expected assuming random
18 assortment ($p < 0.001$; see M&M) (Fig. 3C), which is reminiscent of the observations in
19 circulating immune cell populations (Fig. 1A). This suggests that numerous cell-type specific
20 eQTL also exist in the gut. Accordingly, we observed 524 modules that were only active in
21 one of the 43 cell-types, of which 429 were also location-specific. The latter were mainly eQTL
22 that were active either in enterocytes or their precursors from the small intestine (SI = IL) or
23 in colonocytes or their precursors from the large intestine (LI = TC + RE), respectively (Fig. 3D).
24 We developed a 3D application to visualize the activity of eQTL on a UMAP, vividly illustrating
25 the location- and cell-type-specific activity of some modules (Fig. 3E). For gene-specific
26 modules active in more than one leaf/node, the sign of the eQTL effect was the same in all
27 leaves/nodes for 99.2% of the modules. For 27 genes, however, the effect differed depending
28 on the leaf/node. In a number of instances, this clearly corresponded to a distinct effect
29 depending on cell type (Fig. 3F; STable 13).
30 We then merged intestinal gene-specific modules characterized by similar EAP as measured
31 by θ . These across-gene modules were augmented with 24,333 tier-2 eQTLs (see M&M)
32 recruiting 715 extra genes. This yielded 666 modules encompassing EAP from more than one

1 gene (21.6%), and 2,415 modules that remained monogenic. The number of genes in
2 multigenic modules averaged 2.8, ranging from 2 to 16 (STable 14). The proportion of
3 multigenic modules encompassing eQTL effects with opposite sign was 53%. We observed a
4 number of instances where distinct genes were controlled by the same variants (i.e., were
5 assigned to the same regulatory module) but in distinct cell types (Fig. 3G). All intestinal
6 eQTL/module information in their genomic context is browsable using the same website as
7 for the blood module information (SFig. 7; <https://tools.giga.uliege.be/cedar/publihpg>).

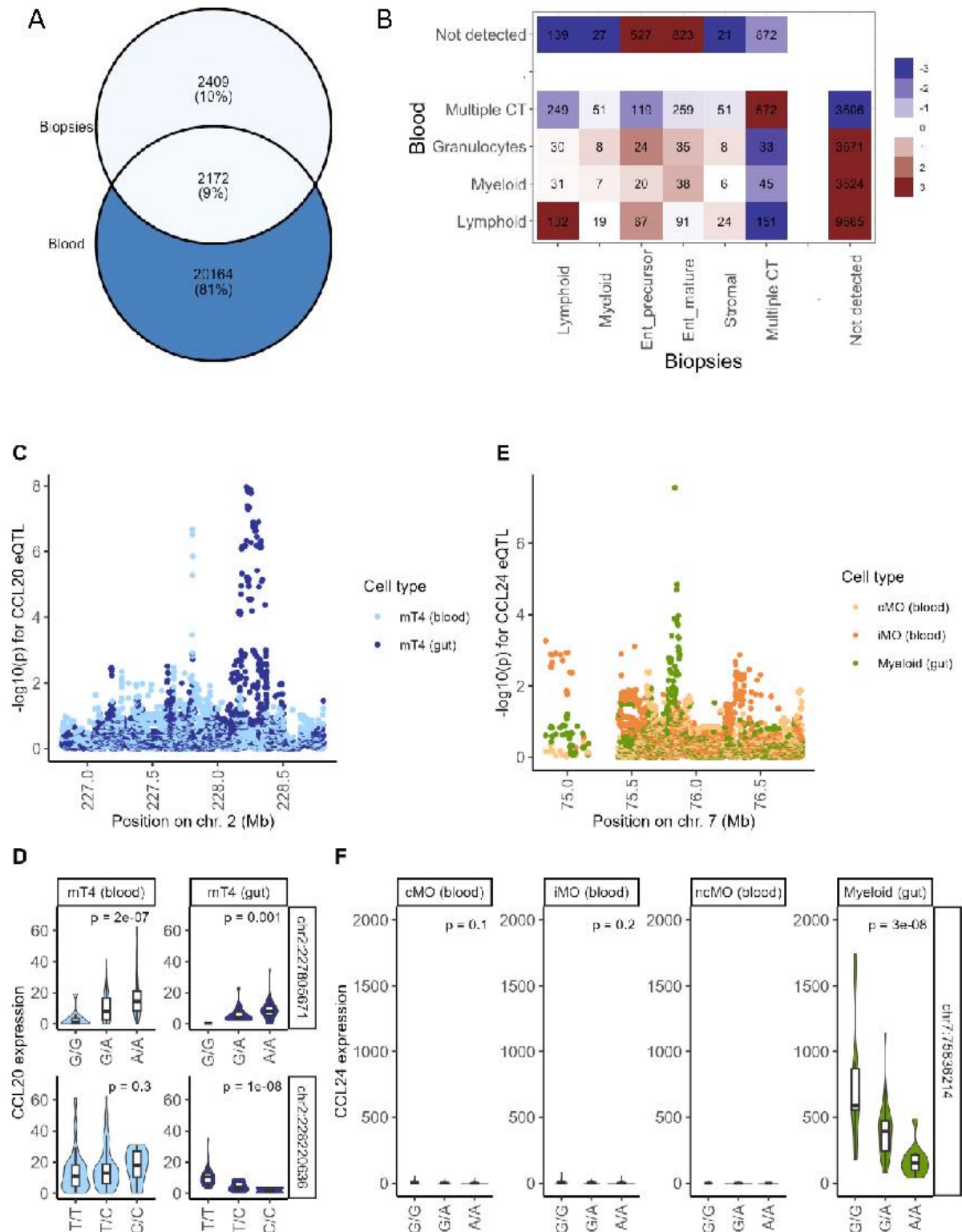
1 assigned. Modules assigned to the root are in dark red, modules assigned to a pair of cell-type categories are in
2 red, modules assigned to one cell-type category are in green (shades of green (from dark to light) correspond to
3 increasing levels of cell-type specificity in the category), modules assigned to a specific anatomical location are
4 shown in blue. The grey distribution was obtained by randomly permuting activity status across modules, yet
5 keeping the number of significant eQTL per leaf/node as for the real data (see M&M). **(D)** Number of modules
6 that are specific for one of the 43 most granular cell-types, whether location specific (IL versus TC+RE) or shared
7 across locations. Cell categories are labeled as before. **(E)** Example of a highly cell type-specific eQTL effect
8 (*GFRA2* in glia (brown)). The x- and y-axes correspond to the UMAP 1 & 2 axes, while the z-axis measures the
9 strength of the association ($\log(1/p)$ multiplied by the sign of β). **(F)** Example of a gene-specific regulatory module
10 (gene: *YEATS4*) for which the sign of the eQTL effects differs between cell types. The module is primarily active
11 in absorptive intestinal epithelium in small (SI = IL, green) and large (LI = TC + RE, orange) intestine. The sign of
12 the eQTL effect switches upon transition from stem/TA cells to precursor enterocytes in both SI and LI. **(G)**
13 Example of two adjacent genes that are controlled by the same *cis*-acting regulatory module yet in different cell
14 types: *SIGLEC12* in enterocytes of the small intestine (SI: green) and *CEACAM18* in enterocytes of the large
15 intestine (LI: orange). The positions on the tree where the RM regulates the corresponding genes are shown as
16 triangles (left panel). The corresponding EAPs and theta-plot are shown (right panels).
17

18 ***Merging blood and intestinal cis-eQTL modules reveals eQTLs that are specific for gut-*** 19 ***resident immune cells***

20 We then merged EAP in regulatory modules using the same approach as before, but this time
21 for the two datasets combined, i.e., blood and biopsies (STable 15 and 16). This yielded 24,745
22 across-gene modules, of which 8,472 were active in more than one cell type. Of the latter,
23 2,172 were found to be active in both blood and biopsies (Fig. 4A). Amongst those, there was
24 a significant excess of modules that were active in multiple cell types in both blood and
25 biopsies ($p < 10^{-5}$), as well as modules that were lymphoid-specific in both blood and biopsies
26 ($p = 7 \times 10^{-4}$). Modules that were active in multiple cell types in the blood had more chance
27 to be detected in biopsies than cell-type-specific blood modules ($p < 10^{-5}$), while modules that
28 were enterocyte-specific in biopsies had less chance to be detected in blood ($p < 10^{-5}$), all as
29 expected (Fig. 4B; Stable 17).

30 We mined the corresponding gene-specific catalog for modules that were labeled lymphoid-
31 or myeloid-specific in biopsies (two cell type categories that are also present in blood), but
32 were reported as “Not detected” in blood. We reasoned that such a list might be enriched in
33 *cis*-eQTL that would not be active in circulating immune cell population(s), but would reveal
34 themselves in the same immune cell population(s) once becoming gut-resident. Hundred-
35 thirty-one modules matched this pattern, of which 57 were dropped after visual inspection
36 of the corresponding EAP using the CEDAR2 website. Of the remaining candidates: (i) 8
37 appeared to be mastocyte-specific eQTL, a myeloid cell type not present in blood, (ii) 39
38 corresponded to genes that were considered to be expressed at too low level in the
39 corresponding circulating blood population to warrant eQTL analysis (and hence likely

1 differentially expressed between cognate circulating and resident cells, and reminiscent of
2 scenario 1 above), and (iii) 26 appeared to be subject to gut-specific eQTL not active in the
3 cognate circulating population despite the genes being detectable (hence reminiscent of
4 scenario 2 above) (STable 18). Thus, it appears that there not only exist many cell-type-
5 specific eQTL, but that – for a given cell type – eQTL can be context specific, f.i. manifest in
6 some anatomical compartments (resident) but not in others (circulating). *CCL20* and *CCL24*
7 constitute two interesting such examples (Fig. 4C-F).



1
2 **Figure 4: Merging regulatory modules across blood and gut samples. (A)** When merging all blood (n=60,113)
3 and gut (n=35,010) eQTL jointly in regulatory modules, we obtained a total of 24,745 cross-gene modules,
4 including 8,472 that are active in several cell types of which 2,172 (9%) encompassed eQTL from blood and gut.
5 **(B)** Modules were assigned to cell types, separately for blood and gut, as described before. Blood cell types
6 were grouped in lymphoid, monocytes/dendritic cells (myeloid), granulocytes or multiple of these cell types (i.e.,
7 active in several of the other categories). Intestinal cell types were grouped in lymphoid, myeloid, enterocyte
8 precursors, mature enterocytes, stromal or multiple of these cell types. “Not detected” indicates that the
9 module is not active in the corresponding sample type (blood or gut). The numbers in the tiles correspond to

1 the number of observations for the corresponding combinations. The colors correspond to $-\log(p)$ of an
2 empirical test of independence (i.e., to what extent do the observed numbers deviate from expectation
3 assuming that the proportions of the different categories in blood and gut are independent). Red: excess. Blue:
4 depletion. **(C)** Example of a gene (*CCL20*, C-C Motif Chemokine Ligand 20) that is expressed in circulating as well
5 as gut-resident memory CD4 T lymphocytes (mT4). However, the gene is subject to two clearly distinct eQTL in
6 these two compartments (light blue: blood mT4 EAP, dark blue: gut mT4 EAP). Of note the EAP observed in
7 circulating cells matches a DAP for UC (Table 21). The corresponding EAP is also detectable in one intestinal mT4
8 leaf, which could very well correspond to blood present in the biopsy. **(D)** Violin plot showing the expression
9 levels of *CCL20* in blood mT4 (left panels in light blue) and gut-resident mT4 (right panels in dark blue) for
10 individuals sorted by genotype for the top SNP of the light blue blood EAP (upper panels) and the top SNP of the
11 dark blue gut EAP (lower panels). **(E)** Example of a gene (*CCL24*) that is strongly expressed in gut-resident
12 myeloid cells (including monocytes and dendritic cells) but nearly undetectable in the equivalent circulating cells
13 (shown for the three types of monocytes: conventional (cMO), intermediate (iMO), and non-conventional
14 (ncMO). *CCL24* is subject to an eQTL that is detectable in gut-resident myeloid cells (green EAP) but not
15 detectable in circulating monocytes (as the gene is virtually not expressed) (yellowish EAP). **(F)** Violin plots
16 showing the expression of the *CCL24* gene in circulating monocytes (three panels on the left), and in gut-resident
17 myeloid cells (panel on the right) for individuals sorted by genotype for the top SNP of the gut EAP in (E).
18

19 **Identifying new *cis*-eQTL driving inherited predisposition to IBD**

20 We then mined our database of blood and intestinal *cis*-eQTL for EAP-matching disease-
21 association patterns (DAP) for inflammatory bowel disease (IBD), with the aim to identify
22 novel candidate causative genes and hence putative drug targets. We defined the boundaries
23 of 206 risk loci reported by Lange *et al.* [2017], encompassing 173 IBD loci (considering CD
24 and UC patients jointly in GWAS), 157 CD loci and 125 UC loci, by visual examination of the
25 local association patterns obtained with (Europeans-only) ~25K cases and ~35K controls
26 from the International IBD Genetics Consortium (IIBDGC) (STable 19). Thirty-two risk loci that
27 encompass composite peaks were further subdivided in sub-risk loci, to be confronted
28 separately to *cis*-eQTL in addition to the cognate complete risk locus. It is indeed conceivable
29 that larger, multi-peak DAP reflect the compound effects of multiple *cis*-eQTL either of the
30 same or different genes in the same or different cell types. Splitting the corresponding risk
31 loci may reveal distinct matching eQTL. Colocalization analyses were conducted using the θ
32 metric, as described in Momozawa *et al.* [2018]. To define suitable thresholds for
33 significance, we performed parallel analyses using permuted genotype data, separately for
34 blood and biopsies (genome-wide *cis*-eQTL analysis in all cell types, leaves and nodes).
35 Confronting results obtained with the real versus permuted data allowed us to compute an
36 FDR for each DAP-EAP pair as a function of the value of $|\theta|$ (≥ 0.6), its *p*-value, as well as the
37 *p*-value (adjusted for *cis*-window) for the eQTL (see M&M). This yielded matching DAP-EAP
38 with $FDR \leq 0.05$ for 379 genes in 119 risk loci (tier-1), or 556 genes in 140 risk loci when
39 considering matching DAP-EAP with $FDR \leq 0.10$ (tier-1+2) (Fig. 5A; Stable 20-22). No credible

1 extra DAP-EAP matches were detected when using the modules' consensus EAP. Of note, and
2 to the best of our knowledge, no eQTL-based connection with IBD has been previously
3 reported for 366 of the 556 genes (STable 22). Matching EAP were detected in both blood
4 and gut for 77 (55%) risk loci, only in blood for 33 (24%), and only in the gut for 30 (21%).
5 Thus, the scRNA-Seq data yielded a comparable number of DAP-EAP matches despite its
6 limited sample size. For risk loci with matching DAP-EAP in both blood and gut, the e-genes
7 involved were generally different. The number of e-genes with matching EAP averaged 4 per
8 risk locus, ranging from 1 to 34 (i.e., for the 140 risk loci with at least one match). Local gene
9 density explained ~25% of the differences in number of matching e-genes per risk locus.
10 There was a strong correlation between the number of matching e-genes in blood and gut for
11 a given risk locus, despite the fact that the genes involved mostly differed (SFig. 8C and 8D).
12 In circulating immune cells, regulatory modules active in all cell types contributed
13 disproportionately to DAP-EAP matches, reminiscent of a previous report [Momozawa *et al.*,
14 2018]. Concomitantly, in biopsies, modules assigned to the root of the tree accounted for the
15 largest proportion of DAP-EAP matches (SFig. 8H and 8I). We note the modest enrichment
16 (1.3-fold) of modules active only in circulating natural killer (NK) cells. Only 12.5% of the 472
17 (= 556 – 84 IBD-only genes) DAP matching e-genes were shared between the two diseases.
18 This proportion only increased to 31.8% when restricting the analysis to the 25 (of 140) risk
19 loci associated with both CD and UC. This possibly underscores the distinct molecular
20 determinism of the two pathologies (SFig. 8 F and 8G).

21 Reactome analysis conducted with the complete gene list highlighted four pathways:
22 interferon gamma signaling (found entities: *CIITA*, *IRF5*, *IRF6*, *PTPN2* and *MHC class I and II*
23 genes), interleukin-6 signaling (*IL6ST*, *IL6R* and *JAK2*), chemokines and their receptors (*CXCR1*,
24 *CXCR2*, *CCR2*, *CCR6*, *CXCL2*, *CXCL5*, *CCL20*), and RUNX regulated immune response and cell
25 migration (*ITGA4*, *ITGAL*) (Stable 23). We scanned the literature, for the 481 protein coding
26 genes out of the list of 556, for functional evidence (other than association or differential
27 expression-based) regarding epithelial barrier function, innate or adaptive immunity that
28 would be considered as support for causality if generated as follow-up of the GWAS and eQTL
29 colocalization. We found such support for 216 of the 556 genes (Table 1; Stable 24 and 25).
30 This included four genes associated with monogenic forms of human inflammatory bowel
31 disease (*CARMIL2*, *PMVK*, *TMEM50B* and *TNIP1*), and 69 genes that upon perturbation affect
32 susceptibility to colitis in a rodent model (Stable 25). The number of genes with incriminating

1 functional evidence averaged 1.46 per risk locus (across the 140 risk loci), with a maximum of
2 15 for the rs3197999 locus on chromosome 3 (48.48-50.23 Mb). There were multiple risk loci
3 with more than one strongly supported candidate gene. For example, the chr1:rs3180018
4 locus harbors the DAP-matching *IL6R* e-gene, member of the inflammatory cytokine pathway
5 highlighted by the Reactome analysis, but also the DAP-matching *PMVK* gene causing IBD-like
6 manifestations in a compound heterozygote [Yildiz *et al.*, 2023]. Along similar lines, the
7 chr5:rs17656349 locus harbors the DAP-matching *IRGM* gene, regulating autophagy and
8 response to various pathogen-associated molecular patterns (PAMPs), and also *TNIP1* coding
9 for the “*TNFAIP3* interacting protein 1”, knowing that *de novo* mutations in *TNFAIP3* are
10 associated with juvenile IBD [Zou *et al.*, 2020; Tanigushi *et al.*, 2021]. Similarly, the
11 chr16:rs28449958 locus encompasses *CARMIL2* causing very early onset IBD [Roncagalli *et al.*,
12 2016; Magg *et al.*, 2019; Bosa *et al.*, 2021], and also *SMPD3*, known to regulate TNF- α
13 response in macrophages and B cells, and to influence the severity of DSS-induced colitis
14 when modulated in mice [Liu *et al.*, 2017; Al-Rashed *et al.*, 2020; Li *et al.*, 2024]. There was no
15 correlation between the number of genes with supporting functional evidence in a risk locus
16 and its odds ratio on disease.

17 Particularly noteworthy is the observation that variants increasing the expression of the cystic
18 fibrosis-causing *CFTR* gene in stromal and/or epithelial precursor cells increase the risk for UC
19 while possibly decreasing the risk for CD (Fig. 5B). This may be related to recent reports that
20 loss-of-function coding variants in *CFTR* protect against CD [Yu *et al.*, 2024]. In addition, we
21 found that variants affecting the expression of *PRKAA1* (shown to phosphorylate and
22 modulate *CFTR* activity [Hallows *et al.*, 2003]), *CDK19* (shown to control the *CFTR* pathway in
23 the intestinal epithelium of mice [Prieto *et al.*, 2022]), *ADCY3* and *PRKAR2A* (both linked to
24 β 2 adrenergic-dependent *CFTR* expression [Belinky *et al.*, 2015]) also affect IBD susceptibility,
25 although these effects were often detected in cells other than the intestinal epithelium. Of
26 note, we observed that variants that decrease *SLC9A3* expression in enterocytes increase UC
27 risk. Loss-of-function mutations in the *SLC9A3* sodium-proton antiporter cause congenital
28 diarrhea 3 and 8 [Dimitrov *et al.*, 2019].

29 Recently, the whole exome of ~30,000 IBD patients was sequenced and rare-variant burden
30 tests (MAF < 0.001) conducted for 11,978 genes [Sazonovs *et al.*, 2023]. The distribution of
31 burden test *p*-values for 298 of our DAP-matching e-genes with sequence information did not
32 depart from expectations under the null (Fig. 5C). Nevertheless, our list of 556 includes

1 TAGAP, one of nine genes with a single associated rare coding variant (as opposed to multiple
2 variants considered jointly in a burden test) identified in this study: a rare missense variant
3 (E147K) protecting against CD (OR: 0.786). TAGAP has an EAP in enterocyte progenitors that
4 matches the DAP of a CD risk locus on chromosome 6 (rs212388) with positive θ (0.79, FDR =
5 0.04), hence compatible with the protective effect of the missense variant. Of note,
6 borderline DAP-EAP hits were observed for two other genes in Sazanovs' list of nine, namely
7 CCR7 (memory CD4 in gut) and RELA (plasmocytes in gut). However, for those two genes the
8 positive sign of θ did, *a priori*, not match the increased risk associated with the reported
9 missense variants. One gene, ATG4C, was further incriminated in this study based on a
10 mutational burden attributed to three missense variants (suggestive signal). ATG4C was not
11 part of our list, but ATG16L2, a paralogue of the ATG16L1 autophagy gene not previously
12 incriminated in IBD, yielded a borderline signal with a convincing θ of 0.77 despite a modest
13 eQTL signal ($p_{window\ adj} = 0.27$).

14 We noticed 10 instances where distinct, cell type-specific EAP from the same gene match DAP
15 from IBD risk loci that were considered different albeit adjacent (QPRT, EIF2B4, TNIP1,
16 PRXL2B, SLC35E2B, IRGM, CDK11B, CD74, SLC25A15, ZNF589). For example, an EAP for IRGM
17 in memory CD8 cells matches the UC DAP in risk locus chr5:rs17656349, while a distinct IRGM
18 EAP in naïve CD4 cells matches the CD DAP in the adjacent chr5:rs11741861 locus. In the
19 same risk locus, a CD74 EAP in colonocyte precursors of the large intestine matches the UC
20 DAP in the chr5:rs17656349 risk locus, while a distinct CD74 EAP in mature enterocytes of the
21 small intestine matches the CD DAP in the adjacent chr5:rs11741861 locus (Fig. 5D). Similar
22 observations were made for multiple sub-risk loci as defined above (STable 22). Thus,
23 complex "composite" disease association patterns may reflect the effect of distinct risk
24 variants that perturb the expression of the same gene in different cell types, with possibly
25 distinct effects on disease. Also, the DAP for CD and UC, even when overlapping and
26 considered as the same risk locus, may differ and match distinct EAP. For example, the CD
27 DAP in risk locus chr6:rs1819333 matches an EAP for RNASET2 that is detected in nearly all
28 circulating immune populations, while the distinct UC DAP in the same risk locus matches a
29 CCR6 EAP active only in NKT cells.

30 We also observed at least 10 e-genes with DAP-matching EAPs in multiple cell types, for which
31 the sign of θ differed between cell types either for the same (CD: FADS1, IL18R1; UC: TOM1;
32 IBD: PRXL2B, UBE2L3) or for different forms of IBD (CD74, IL1R2, IRGM, PRXL2B, CD244

1 (=SLAMF4), SLC25A15) (f.i. Fig. 4D). This calls for caution when defining the desired effect of
2 a drug (activator or inhibitor) based on the sign of θ .

3 The CEDAR2 web-site [<https://tools.giga.uliege.be/cedar/publihpg>] allows for convenient
4 visual inspection of the matching DAP-EAP patterns underpinning our analyses as well as
5 downloading of the data.

6

7 **Entrectinib, a small molecule NEK7 inhibitor, is a repurposing candidate for IBD**

8 It is not obvious that pharmacological targeting of causative genes (that upon perturbation
9 by common regulatory variants increase the chance to develop the disease), will succeed in
10 reversing the disease process once initiated, i.e., be curative. Additional prioritization of
11 candidate genes whose expression is also perturbed by the disease process itself may be
12 useful. To that end we collected blood from 55 active CD patients, performed RNA-Seq on
13 the same 27 fractionated circulating immune cell populations, and performed differential
14 expression analysis between the two cohorts (cases vs controls) by cell type (STable 26). We
15 additionally consulted lists of genes that were shown, from scRNA-Seq data, to be
16 differentially expressed between intestinal biopsies of IBD cases and controls [Kong *et al.*,
17 2023], as well as lists of proteins that were differentially abundant in plasma of IBD cases and
18 controls [Eldjarn *et al.*, 2023]. The expression of 109 of our 556 e-genes differed in cases in a
19 manner that was consistent with the sign of θ (i.e., both risk variant and disease increase
20 expression, or both risk variant and disease decrease expression) in one of the three data sets
21 (circulating immune populations, biopsies or plasma), of 40 e-genes in two of the three data
22 sets, and of three e-genes in the three data sets (circulating immune populations and biopsies
23 and plasma) (Fig. 5E).

24 Hundred eighty-one drugs targeting 180 e-genes are or have been used/tested to treat IBD
25 [Mountjoy *et al.*, 2021; Vieujean *et al.*, 2024] (STable 27). Eleven of these overlapped with
26 our list of 556 e-genes: CXCR2 (elubrixin: abandoned for lack of efficacy), IL6R (TJ301: phase
27 2 ongoing), IL6ST (olamkicept: phase 2 completed with positive results), IMPDH2
28 (mycophenolate: abandoned for undocumented reasons), ITGA4 (multiple in phase 2 and two
29 approved including vedolizumab), ITGAL (efalizumab: abandoned for safety issues including
30 multifocal leukoencephalopathy), JAK2 (multiple with positive results after phase 2 for
31 peficitinib), NDUFAF1 (metformin: phase 2 ongoing), PDCD1 (rosnilimab: phase 2 ongoing),
32 TEC (ritlecitinib: phase 2 completed with positive results for CD and UC) and TNFSF15 (several:

1 phase 2 ongoing) (STable 22). For seven of these (*IL6R*, *IL6ST*, *ITGA4*, *ITGAL*, *JAK2*, *IMPDH2*,
2 *PDCD1*), the effect (presumed activator vs inhibitor) of at least some of the drugs was in
3 agreement with the sign of θ . For six (*CXCR2*, *IL6ST*, *IL6R*, *ITGAL*, *JAK2*, *NDUFAF1*), the effect
4 of disease on expression/abundance level was compatible with the effect of the drug (STable
5 22). We further identified another 40 genes in our list of candidates, targeted by known drugs
6 (in phase 1 or higher) that – to the best of our knowledge – have not been tested in the
7 context of IBD (STable 22). For 16 of these the activity of at least one drug (likely inhibitor or
8 activator) was consistent with the sign of θ . The corresponding drugs were in phase 1 for two
9 (*PIM3*, *RPS6KB1*), phase 2 for six (*ATP2A1*, *CDK11B*, *ERAP2*, *HLA-DRB1*, *KIR2DL1*, *PPP5C*),
10 phase 3 for one (*INPP5D*), and approved for at least one disease other than IBD for seven
11 (*CFTR*, *CYP3A5*, *IL18R1*, *IL18RAP*, *LAMA2*, *NEK7* and *PTGIR*). For 6 of the 16 genes
12 (underlined), expression was predominantly affected by the disease process in a manner
13 consistent with θ , at least in one of the three datasets. Detailed examination of the drugs
14 that were in phase 3 or higher (Supplemental Material 1), identifies entrectinib (ENB) as a
15 possible repurposing candidate for IBD. Entrectinib (ENB) is a potent tyrosine multikinase
16 small-molecule inhibitor that targets the NTRK, ROS1 and ALK oncogenes, approved by the
17 FDA for the treatment of various tumors [Liu et al., 2018]. It was recently shown to bind to
18 arginine 121 of NEK7, thereby inhibiting its interaction with NLRP3 [Jin et al., 2023].
19 Downregulation of *NEK7* by intraperitoneal injection of lentiviruses expressing anti-*NEK7*
20 shRNAs was shown to attenuate DSS-induced colitis [Chen et al., 2019]. In mouse models, ENB
21 effectively reduced symptoms of NLRP3 inflammasome-related diseases (other than colitis)
22 [Jin et al., 2023]. ENB has a high safety profile and is well tolerated by almost all patients
23 without cumulative toxicity [Jiang et al., 2022]. Genetic variants that increase *NEK7*
24 expression in naïve B cells increase the risk for IBD ($\theta=0.94$; FDR=0.02), while *NEK7* expression
25 is increased in a majority of circulating immune cells of active CD patients, and in non-
26 inflamed colonic epithelium of CD patients when compared to controls [Kong et al., 2023].
27 On the downside, there is some evidence, albeit non-significant, that the same genetic
28 variants decrease *NEK7* expression in some gut-resident immune cells
29 (<https://tools.giga.uliege.be/cedar/publihpg>), while *NEK7* expression is up-regulated in some
30 circulating immune cells of active CD patients (f.i. eosinophils, Stable 22).

31

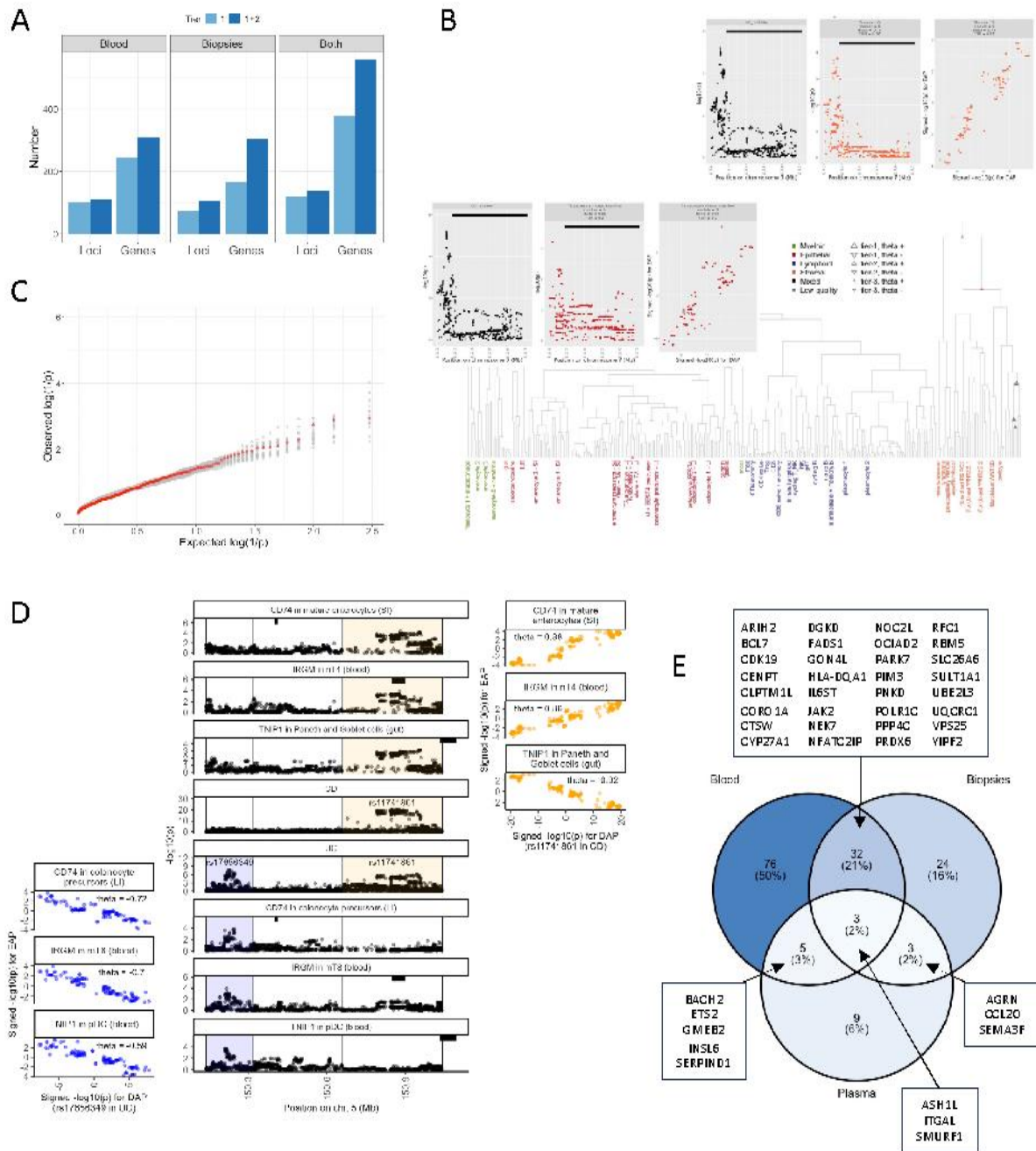
32

1

2 **Table 1:** List of 211 e-genes with DAP-matching EAP and published evidence (documented in STable 25 and
 3 Suppl. Material) for an effect on one or more functions in one or more cell types participating in epithelial barrier,
 4 innate and adaptive immunity, or other IBD-relevant mechanisms. Genes affecting multiple categories of
 5 functions are italicized.

Function	Genes
Epithelial homeostasis & barrier function	Epithelial transporters <i>ABCC2, ADCY3, CDK19, CFTR, MFSD4B, PRKAA1, PRKAR2A, SLC5A6, SLC9A3</i>
	Epithelial integrity & repair <i>CD74, CDH3, CERS2, CTSX, ERBB2, HSPD1, INAVA, IRF6, KSR1, LASP1, MASTL, PAR6A, PEX6, PLA1, RAB13, TKT, ZEB2-AS1</i>
	Epithelial stem cells & development <i>CDX1, HSPG2, LAMA2, NRBP1, SETDB1, SRCAP</i>
Signalling in innate immunity	Pathogen-recognition receptors <i>ANKRD17-DT, ARIH2, ATG16LI, CARD9, CYLD, IL1R1, IL1R2, IL18R1, IL18RAP, INAVA, IPMK, IRF5, IACCI, LAMA2, NEK7, ORMDL3, PRKDC, RFTN2, RNASET2, RNFI23, SEC24C, SSC5D, SENP7, TRAF3IP3, TRAIIP, TRIM37, IRGM, UBR2, USP19, ZC3H15, ZDHHC11B, ZFP91</i>
	TNF signalling <i>ADCY7, BABAM2, LTBR, MST1, MST1R, RASSF1, TNFRSF14, TNFRSF9, TNFSF15, TRAIIP, ZFP36L2</i>
	JAK-STAT signalling <i>FAM220A, JAK2, OOAD2, PRKAR2A, PTPN2, TYK2</i>
	IL6, SLAMF, Others <i>ASH1L, DGKD, EDC4, IL26, IL6R, IL6ST, Lya, OSM, RASGRP1, SLMAF1, SLMAF4</i>
Cells in innate immunity	Leucocyte extravasation & trafficking <i>CDH26, CORO1A, CXCR1, CXCR2, CXCL2, CXCL5, CXCL1, CXCL8, GCA, ITGA4, ITGAL, LSP1, NEU4, SEMA3F, TLN1, TMEM87A, TSPAL7</i>
	Macrophages <i>ALUJ, CCR2, ETS2, LACCI, PPM1F, PROK2, QPCTL, SMPD3, SPI40</i>
	Other or multiple myeloid cells <i>ARNT, FOXP1-AS1, HINT1, INPP5D, KIR3DL1, KIR3DL3, PLPP6, PPP3CB</i>
Autophagy & ubiquitin-dependent processes	Autophagy <i>ATG16LI, CDK11B, CLTC, CORO1A, CUL1, DAP, IPMK, IRGM, NR1D1, PGNP, PIM3, PPP3CB, PTPN23, SHSAS, TFAM, TUFM, USP19, VPS37C</i>
	Ubiquitin-dependent processes <i>BBC3, CSID1, CUL2, FBXL19, KBTBD6, LTBR, MIB2, OTUD7B, PLA2G15, QRICH1, RNFI23, SEC24C, SMURF1, TOM1, UBE2L3</i>
Other inflammation mediators	Prostaglandins & glucocorticoids <i>FADS1, FADS2, HSD11B1, PTGIR, PRXL2B, PRKAR2A</i>
	Complement system <i>CD46, CR2, GNA12</i>
Antigen presentation & MHC	<i>CD74, CIITA, CTSS, ERAP2, LNPEP, RFX5, (+MHC)</i>
Signalling in adaptive immunity	BCR &/or TCR <i>CD19, LAT, LIME1, PTPRC, PTPRH, RFTN2, SLAMF8, THEMIS, TRAF3IP3</i>
	CCR6, Others <i>ADCY7, CCL20, CCR6, DGKD, DUSP8, ELF3, Lya, RASGRP1, SH2B3, SLAMF4</i>
Cells in adaptive immunity	T cells <i>ATXN2L, BCL2L12, CCR2, CORO1A, CREM, CTSX, CTSW, FOSL2, GMEB2, GSDMB, MED1, NFATC2IP, PDCD1, PDXN1, PPP3CB, PPP4C, SEMA3G, TAGAP, TEC, TKT, USP4</i>
	B cells and multiple <i>BACH2, BRWD1, HHEX, IKZF3, INPP5D</i>
Other	Other mechanisms <i>COQ10B, CYP3A5, FUT2, GPXL, HYAL1, UGI1, NADK, OAT, QPRT, RXFP4, SLC22A5, SLC25A15, SPI40, SPHK2, TAS1R3, THRA</i>
	Monogenic forms of IBD <i>CARMIL2, PMVK, TMEM50B, TNIP1 (per TNFAIP3)</i>

6



1
2 **Figure 5: (A)** Numbers of IBD risk loci and genes identified with matching DAP-EAP in the 27 circulating immune
3 cell populations (blood), in the 43 intestinal cell populations (biopsies), and when combining both datasets
4 (Both). Tier 1 corresponds to matching DAP-EAP with $|\theta| \geq 0.6$ and $FDR \leq 0.05$. Tier 2 corresponds to matching
5 DAP-EAP with $|\theta| \geq 0.6$ and $0.05 < FDR \leq 0.10$. **(B)** EAP of the cystic fibrosis *CFTR* gene matching the DAP of
6 a UC risk locus on chromosome 7 (rs38904) in secretory TA precursor cells (red) and intestinal stromal cells
7 (orange). The nodes/leaves with DAP-matching EAP are marked by triangles (large: $FDR < 0.10$, small: $FDR >$
8 0.10). Insets: (left) DAP for UC, (middle) EAP for *CFTR*, (right) θ plot, (red) secretory TA precursor cells, (orange)
9 stromal cells. The boundaries of the *CFTR* gene are marked by the thick horizontal black line. The positive sign
10 of θ indicates that downregulation of the *CFTR* gene in these cell types may be protective, which is corroborating
11 the recent finding that *CFTR* loss-of-function mutations protect against CD [Yu *et al.*, 2024]. **(C)** QQ plot
12 generated with the burden test p-values obtained for 298 of our 556 DAP matching e-genes by Sazonovs *et al.*
13 [2022] (red dots). Grey dots correspond to QQ plots obtained with randomly sampled sets of 298 genes from
14 the list of genes with data in Sazonovs *et al.* [2022]. **(D)** Central panel: DAP for CD and UC in two adjacent risk
15 loci on chromosome 5 (rs17656349 shaded in blue, and rs11741861 shaded in yellow), as well as (below) EAP
16 matching the rs17656349 UC DAP for *CD74* (colonocyte precursors in large intestine), *IRGM* (circulating memory

1 CD8), and *TNIP1* (circulating plasmacytoid DC), and (above) EAP matching the rs11741861 CD/UC DAP for *CD74*
2 (mature enterocytes in small intestine), *IRGM* (circulating naïve CD4), and *TNIP1* (paneth and goblet cells). The
3 genomic position of the corresponding genes are marked by black horizontal bars. The corresponding theta
4 plots are shown on the left (rs17656349 in blue) and right (rs11741861 in yellow), respectively. **(E)** DAP matching
5 e-genes whose expression levels are affected by the IBD disease process in a direction that is consistent with the
6 effect of risk variants (i.e., both risk variant and disease increase expression, or both risk variant and disease
7 decrease expression) in one or more of 27 circulating immune populations (Blood), in intestinal biopsies
8 (Biopsies, Kong *et al.*, 2023), or in plasma (Plasma, Eldjarn *et al.*, 2023).
9

10 Discussion

11 **Regulatory modules: sensible (e)QTL analysis framework?** It is generally admitted that most
12 CCD risk variants act by perturbing the expression of causative genes in one or more disease-
13 relevant cell types, and that it should be possible to pick-up many of these regulatory effects
14 as *cis*-eQTL in these cell types. *Cis*-eQTL effects are pervasive and it is therefore not sufficient
15 to identify a *cis*-eQTL overlapping a risk locus to assume that it affects risk. By definition,
16 causal *cis*-eQTL are determined by the same variant(s) that affect disease risk. As a
17 consequence, the pattern of association between regional variants and gene expression (EAP)
18 should be the same as that for the disease (DAP). This is certainly the case if disease and gene
19 expression are measured in the same individuals. It is also the case if disease and gene
20 expression are measured in distinct cohorts, provided that they share local LD structure. The
21 DAP-EAP similarity applies to the causal variant(s) *per se*, but also to passenger variants whose
22 association with disease and gene expression is indirect, reflecting their LD with the causative
23 variant(s). The expression of a given gene may be controlled by distinct sets of regulatory
24 variants in distinct cell types. This will yield distinct EAP for the same gene, even if the
25 respective sets of regulatory variants partially overlap. The DAP will only match the gene's
26 EAP in the disease-relevant cell type. It is conceivable that the expression of a causal gene in
27 more than one cell type (with distinct EAP) influences disease risk. If the significant variants
28 for the corresponding EAP are sufficiently distant, multiple DAP-matching EAP may be found
29 for the same gene in different cell types. We have observed several such instances in this
30 work, for adjacent sub-risk loci or even adjacent risk loci considered separate thus far (f.i. Fig.
31 5D & STable 22). We have also observed instances where distinct EAP (corresponding to
32 different cell types) for the same gene match the DAP for different diseases (in this case CD
33 and UC). If the significant variants of the distinct EAP overlap, the DAP may not match either
34 EAP. More advanced approaches would be needed to dissect such cases, converging towards

1 fine-mapping of multiple independent variant effects. This, however, requires larger sample
2 sizes than what is presently available for multi-tissular eQTL studies.

3 Causal *cis*-eQTL are the first links in the chain connecting risk variants with disease, the final
4 outcome. The same regulatory module-based approach can in theory be used to uncover the
5 intermediate molecular links between risk variants and disease, provided that the abundance
6 or state of the corresponding molecular species can be quantified. The corresponding *trans*-
7 QTL (whether expression QTL or any other quantifiable molecular phenotype) should be
8 characterized by DAP-matching EAP. CCD are highly polygenic, influenced by hundreds of risk
9 loci or more. It is likely that at least some pathways linking variants with disease converge
10 prior to disease outcome. Thus, some intermediate molecular phenotypes will have matching
11 EAP with multiple DAP (distinct risk loci). This should allow reconstruction of the topology of
12 the pathways linking the multiple risk variants with the disease.

13 ***Cell-type specificity of regulatory modules operating in immune cell populations.*** One
14 striking observation of this work, is that 73.2% of blood regulatory modules were found to be
15 active in only one of the 27 studied immune cell populations. Most of the time (100-
16 8.5=91.5%) the corresponding genes did not appear to be under marked genetic *cis*-control
17 in the 26 other cell types (i.e., no module switch). Hence, a large proportion of eQTL appear
18 to be very cell-type specific at the chosen level of granularity, at least in blood. One could
19 argue that this is a power issue: the eQTLs may have existed in some other cell type, but
20 remained under the radar of statistical significance because of insufficient sample size. We
21 therefore expanded our search for matching EAP to non-significant eQTL, i.e., we allowed for
22 tier-2 eQTL to enter into the modules if their EAP matched significant ones with $|\theta| \geq 0.6$ and
23 a combination of *p*-values of match and eQTL ensuring an FDR ≤ 0.05 (see Results and M&M).
24 This had virtually no effect on the proportion of modules that were active in only one cell type
25 (from 76% to 73.2%). We therefore think that the observed eQTL cell-type specificity is
26 genuine. These findings are reminiscent of those reported in circulating immune cells by
27 Schmiedel *et al.* [2018] and Ota *et al.*, [2021], and across multiple tissues by the GTEx
28 consortium [2020].

29 The eQTL specificity may even be more pronounced for at least some immune cell
30 populations, being in addition context-dependent. Indeed, the availability of scRNA-Seq data
31 for intestinal biopsies allowed us to compare eQTL activity for the same cell type yet
32 circulating in blood on the one hand, and resident in the intestine on the other hand. To

1 detect such compartment-specific eQTL, we focused our attention on modules that were
2 significantly active in (i) lymphocytes, or (ii) macrophages/monocytes/dendritic cells isolated
3 from the intestinal biopsies, but not in the equivalent cell types isolated from blood. We
4 didn't add the mirror comparison, i.e., modules active in blood but not in gut, because we
5 assumed that we had more (statistical) power to detect eQTL in blood than in gut. The
6 absence of a detectable eQTL effect in the gut could more often be a trivial power issue. We
7 detected several instances supporting the existence of such compartment-dependent eQTL
8 (STable 18). Part of these seem to involve induction of gene expression upon entering the
9 intestinal compartment (scenario 1), others seem to be independent of gene expression level
10 but a genuine conditional effect of the regulatory variants (scenario 2). We illustrate both
11 scenarios using *CCL24* in monocytes/macrophages and *CCL20* in T lymphocytes, two CC-motif
12 chemokines with chemotactic and antimicrobial activity whose genes show to have higher
13 expression and be under specific genetic *cis*-control in the gut (Fig. 4C and 4D).

14 ***Using inferred cell-type ontogeny to effectively map eQTL using scRNA-Seq data.*** Obviously,
15 the observed degree of eQTL cell type specificity will depend on the chosen cell type
16 granularity. This becomes particularly pertinent when working with single cell (ultimate
17 granularity) RNA-Seq data: if one splits a cell cluster in sub-clusters, what was an eQTL specific
18 for the cluster may now become shared by the sub-clusters (and hence apparently less cell
19 type specific). Deciding at what cluster resolution to perform eQTL analysis will also have a
20 considerable impact on eQTL detection: considering two clusters that share an eQTL
21 separately rather than together, may decrease the detection power if the number of cells in
22 each cluster is power limiting. The optimal cell partitioning strategy to detect a given
23 eQTL/module will depend on where (i.e., in which cell types) the eQTL/module is active. If an
24 eQTL is active in all cell types, the best strategy is to consider all cells jointly. If an eQTL is
25 specific to a very small subset of cells, merging these cells with others that do not express the
26 eQTL will reduce detection power. To address these issues in a generic way, we decided to
27 construct a hierarchical tree of cell clusters based on the similarity of their transcriptomes.
28 We assumed and demonstrated that this tree largely reflects cellular ontogeny. We also
29 assumed that regulatory modules are turned on at specific developmental stages (i.e., nodes
30 or leaves of the tree) and affect at least part of downstream branches along variable length.
31 Accordingly, we performed eQTL analysis separately for all leaves and nodes of the tree. This
32 effectively guides and limits the cell pooling options in an ontogenic framework, yet allows

1 informed exploration of many possible scenarios. Of note, the proposed method disconnects
2 eQTL mapping from cell type annotation.

3 The eQTL detection step was followed by the merging of similar EAP into modules, and the
4 visualization of where a given module is active along the hierarchical tree (see f.i. Fig. 3F).
5 Assuming that the module has been turned on once along the ontogenic tree, the signal
6 should be the strongest for the node corresponding to the ontogenic stage where it was
7 turned on. The signal should become weaker as one moves towards the root as the cells in
8 which the module is active are progressively diluted by cells in which it is not. It should also
9 become weaker as one moves towards the leaves as the number of cells for analysis
10 decreases. Thus, one could assign the module to the segment in the tree where the detection
11 signal is maximal. In reality we didn't see the predicted smooth decrease of signal strength
12 up and down-wards (in the tree) from a point of maximum significance, presumably because
13 signal strength is affected by a multitude of other factors. We therefore chose to assign the
14 module to the most recent common ancestor (MRCA) of all active leaves/nodes, which may
15 result in positioning the modules too much towards the root.

16 The number of nodes/leaves in which modules were active showed a clear sign of
17 overdispersion with many modules being either active in fewer nodes/leaves than expected
18 by chance, or active in more nodes/leaves than expected by chance. As for blood, the excess
19 of modules active in fewer than expected nodes was unlikely due to statistical power issues
20 as augmenting modules with matching yet less significant eQTL didn't affect this pattern. We
21 believe that this indicates that many regulatory modules are cell type specific in the gut as
22 previously observed for the FACS/MACS sorted circulating immune cell populations. In
23 particular, enterocytes and stromal cells from the small intestine differ considerably from
24 those of the large intestine, both with regards to transcriptome (Fig. 2E) and eQTL activity
25 (Fig. 3D).

26 ***Increasing cell-type granularity uncovers new IBD-driving regulatory modules.*** The initial
27 premise of this work was that a large fraction of risk loci remained "orphan" thus far, because
28 the disease driving-eQTL were active in cell types that were absent or underrepresented in
29 previous eQTL datasets. The observation that a large fraction of eQTL/modules indeed
30 appear to be highly cell type and even context specific supports this hypothesis. Accordingly,
31 this work in essence doubles the number of IBD risk loci with DAP-matching eQTL to 140, i.e.,
32 ~70% of the 206 studied risk loci. For approximately half of risk loci (55%), DAP-matching

1 EAP were detected in both blood and gut. For the remaining half, there were slightly more
2 matches in blood (24%) than in the gut (21%). Thus, scRNA-Seq-based eQTL detection in the
3 gut made a considerable contribution to DAP-EAP matching despite the fact that we analyzed
4 samples from only 57 individuals (yet in three locations). It seems reasonable to assume that
5 increasing intestinal scRNA-Seq sample size will uncover DAP-matching EAP for additional risk
6 loci, and meta-analyses towards that goal are in progress.

7 An additional factor that has contributed to the marked increase in the number of IBD risk
8 loci with DAP-matching EAP is the splitting of risk loci into sub-risk loci. This was done for 32
9 of the 206 studied risk loci, because we assumed that “multimodal” DAP might be the sum of
10 multiple independent EAP. This strategy allowed us to detect an extra 28 DAP-matching e-
11 genes, covering an additional nine IBD risk loci.

12 It has been argued that it may be more effective to perform eQTL analyses in fewer, easily
13 collectable sample types (f.i. whole blood) but from many more individuals, than to increase
14 sample types yet remain limited in the number of individuals, to uncover more DAP-matching
15 EAP. To verify this, we used PBMC eQTL summary statistics from ~30,000 healthy individuals
16 of European descent [Vösa *et al.*, 2021], and searched for DAP-matching EAP using a slightly
17 more permissive procedure as the one used with our own expression data. Using Vösa’s data,
18 we identified DAP-matching EAP for 39 loci involving 59 genes. Using our own PBMC
19 information (i.e., 187 individuals), we identified DAP-matching EAP for 32 IBD risk loci
20 involving 42 genes, with 12 overlapping loci and three overlapping genes. Using our full blood
21 data set (27 immune cell populations), we identified DAP-matching EAP for 110 loci involving
22 310 genes, of which 36 loci and 27 genes overlapping with Vösa. Using our complete data
23 set (blood and gut), DAP-matching EAP for 140 loci involving 556 genes, of which 38 loci and
24 30 genes overlapping with Vösa. Thus, the Vösa data enabled the identification of matching
25 EAP for one IBD risk locus (rs1479918), and 29 e-genes that were missed with our data.
26 However, we identified matching EAP for 102 IBD risk loci, and 526 e-genes that were missed
27 with Vösa’s data. These findings suggest that a large number of additional matches are
28 uncovered when performing eQTL analyses in isolated cell types.

29 ***Are the e-genes controlled by IBD-driving regulatory modules causal?*** The initial
30 assumption, when eQTL studies to identify causative genes in risk loci were initiated, was that
31 DAP-matching EAP would occur rather exceptionally, yet - when detected - would provide
32 strong evidence for gene causality. It now appears that DAP-matching EAP are rather

1 common, and that for many risk loci, DAP-matching EAP are found for multiple genes (STable
2 21&24). Moreover, we find in this work that when, for a given risk locus, DAP-matching EAP
3 are found in both blood and gut, the genes involved are largely different. Are all of these
4 genes, one way or the other, causally involved in disease risk, only some, or none? In other
5 words, what is the proportion of “red herring” eQTL [Connally *et al.*, 2022] amongst DAP-
6 matching EAP? All scenarios are plausible, and each one likely applies to at least some risk
7 loci.

8 It seems possible that - because *cis*-acting regulatory elements are often shared by multiple
9 genes [f.i. Thurman *et al.*, 2012] – many regulatory variants will affect the expression of
10 neighboring genes including some that have no bearing on disease risk. The relatively modest
11 signals obtained by pathway enrichment analyses (STable 23) supports the assertion that a
12 sizable proportion of DAP-matching e-genes are not directly influencing disease risk. It is
13 tempting to assume that DAP-matching information will be more specific for risk loci with
14 fewer matching e-genes, and this information is available from STable 21&24.

15 On the other hand, when scanning the literature for functional evidence supporting the causal
16 involvement of genes in our candidate list, we were struck by the large number of DAP-
17 matching e-genes with such evidence (212 out of the 483 examined coding genes). Several
18 risk loci harbor more than one gene with quite enticing support (see examples, in results, of
19 loci with strong functional candidates that additionally harbor less well-known genes
20 underpinning early onset, Mendelian forms of IBD). Thus, it seems likely that – at least for
21 some risk loci – the risk variants are affecting the expression of multiple genes that jointly
22 affect the risk to develop IBD. In other words, the notion of polygenicity may not be limited
23 to the fact that disease risk is affected by multiple loci in the genome, but additionally that
24 (at least some) risk loci harbor multiple causative genes controlled by the same or distinct
25 regulatory modules. An additional level of complexity may result from the fact that a single
26 gene may affect disease outcome through multiple pathways, operating for instance in
27 different cell types, triggered by the same or by different regulatory modules. For example,
28 *INAVA* was shown to play a pivotal role in PRR-induced signaling, cytokine secretion and
29 bacterial clearance in peripheral macrophages and intestinal myeloid cells [Yan *et al.*, 2017],
30 yet at the same time to regulate the stability of adherens junctions of intestinal epithelial cells
31 (where we see the best DAP-match) [Mohanam *et al.*, 2018]. Also, *ATG16L1* is increasingly
32 understood to affect disease outcome through autophagy-dependent but also -independent

1 mechanisms [Hamoui *et al.*, 2022], in agreement with our observation of a DAP-match in
2 eosinophils but also colonocyte precursors. The suggestion that specific risk loci may affect
3 disease outcome through multiple genes and pathways is also well illustrated by the
4 *CCR6/RNASET2* and *IRGM/CD74/TNIP1* gene sets.

5 Is it possible that for some risk loci, none of the DAP-matching e-genes are causal? Positional
6 cloning has been pursued very successfully during the last 30 years, under the assumption
7 that causative mutations always affect the function of a causal gene in *cis*. A key assumption
8 of the omnigenic model [Boyle *et al.*, 2017; Liu *et al.*, 2019] is that variants can affect
9 phenotype without having any causal *cis*-effect on the expression of neighboring genes. That
10 doesn't mean that one will not see *cis*-eQTL effects on neighboring genes, but rather that
11 these do not influence the phenotype: a sobering thought for positional cloners.

12 Of note, we didn't see an effect of the number of DAP-matching genes, with or without
13 reported function, per risk locus on the magnitude of its effect on disease (measured by the
14 odds ratio (OR)). This is not surprising given that many factors will affect OR, but a positive
15 result would have been in support of the "multigenic" nature of individual risk loci whether
16 being causal *per se* or not (i.e., omnigenic model).

17 ***Are multi-genic and multi-tissular regulatory modules underpinning pleiotropy?*** The
18 number of DAP-matching e-genes is remarkably high for some risk loci, often despite any
19 obvious functional theme or coherence. This suggests that risk variants may hit master *cis*-
20 regulators that control the expression of large chromosome domains and many genes therein,
21 irrespective of function. We reasoned that such variants might, because of the number of
22 affected genes, influence multiple traits, i.e., be pleiotropic. Of interest, under this scenario,
23 the mechanism accounting for pleiotropy would only involve the variants, not the e-genes
24 affected in *cis*, as causative genes would differ between traits. It is well established that as
25 many as 90% of GWAS-identified risk loci affect multiple traits, that can even belong to
26 distinct "trait domains". We searched for a correlation between the number of DAP-matching
27 (IBD) e-genes and the number of trait domains pleiotropically affected by the corresponding
28 risk loci as reported in Watanabe *et al.* [2019] (SFig. 8C). There was no obvious relation
29 between these two statistics. Thus, at first glance, it does not seem that risk loci with high
30 numbers of DAP-matching e-genes make a disproportionate contribution to pleiotropy.

31 Regulatory modules that are active in all cell types, make a disproportionate contribution to
32 the risk loci with DAP-matching EAP, particularly in blood (SFig. 8H and 8I). We made a similar

1 observation for IBD risk loci with the less-granular CEDAR1 data set [Momozawa *et al.*, 2018].
2 This is possibly due to the fact that detecting the DAP-match is less dependent on analyzing
3 the correct (i.e., disease-relevant) cell type for these risk loci.

4 ***Why are DAP-matching e-genes not showing an excess burden of coding variants in***
5 ***patients?*** As discussed before, being a DAP-matching e-gene does not prove that it is causally
6 involved in disease risk. There are two formal tests of gene causality. The first is the reciprocal
7 hemizyosity test, which is very difficult to apply in mammals, let alone humans [Steinmetz
8 *et al.*, 2002; Stern *et al.*, 2014]. The second is the enrichment of disruptive coding variants in
9 cases. For example, this test was used to demonstrate the causality of *NOD2* in CD [Hugot *et*
10 *al.*, 2011; Lesage *et al.*, 2002]. Therefore, a logical next step after the identification of DAP-
11 matching e-genes, is to sequence the corresponding genes in large case-control cohorts and
12 to perform rare variant-based burden tests [f.i. Momozawa *et al.*, 2018]. As a matter of fact,
13 this approach has now been applied genome-wide (i.e., without preselection of target genes
14 using eQTL information) for several common complex diseases on very large cohorts including
15 IBD [Sazanovs *et al.*, 2022]. Although some new causative genes have been identified using
16 this approach (including some that overlap with DAP-matching candidates, including from this
17 study), the yield has been, arguably, somewhat disappointing given the magnitude of the
18 effort. The same applies to most diseases for which this approach has been used [f.i. Flannick
19 *et al.*, 2019]. We herein have used Sazanovs' resequencing data to look for the distribution
20 of burden test *p*-values for 298 candidate e-genes out of our list of 556. There was no
21 evidence from a departure from expectation under the null (Fig. 5C). Does that mean that
22 none of our DAP-matching e-genes are affecting IBD risk? Although we cannot completely
23 exclude that possibility, alternative explanations exist. One is a power issue: sequencing
24 35,000 cases is a lot but may not be sufficient, especially for small genes, and given the fact
25 that predicting the effect of coding variants other than stop-gains remains difficult. The other
26 is that coding variants in the corresponding genes do not cause IBD but possibly other
27 diseases. A fundamental difference between coding and regulatory variants is that coding
28 variants affect the function of the gene equally in all tissues where the gene is used, while
29 regulatory variants likely affect the function of the gene in a restricted set of tissues. It is
30 increasingly apparent that most genes are utilized in many tissues and cell types, as testified
31 by the many synonyms existing for most gene names. As indicated by their denomination,
32 diseases such as IBD are organ-restricted in their manifestations. It is very possible therefore

1 that to be risk variants for IBD the effects have to be organ restricted (gut and immune cells),
2 and that – for many genes - this does not apply to coding variants. The target space to
3 resequence may therefore have to be redirected to (cell type-specific) *cis*-acting regulatory
4 elements, yet these remain difficult to identify, the effects of variants on their functionality
5 difficult to predict, and the corresponding genome space limited (hence affecting power).

6 **Genetic support for new repurposing opportunities in IBD.** We identify entrectinib as a
7 promising repurposing candidate for CD. Entrectinib (ENB) is a small molecule that blocks
8 several tyrosine kinases including oncogenic ones. It has been approved by the FDA in 2019
9 for the treatment of several solid tumors. It is administered orally and has proven safe and
10 well tolerated even at high doses and prolonged administration. More recently, a screening
11 of FDA-approved kinase inhibitors, showed that ENB specifically blocks the NLRP3
12 inflammasome. This was shown to result from the reversible binding of ENB to R121 of the
13 NEK7, thereby inhibiting NLRP3 activation. Paradoxically, ENB does not affect NEK7's kinase
14 activity, which increases the effect's specificity. *In vivo* tests show that shRNA-mediated
15 downregulation of NEK7 protects mice against DSS-induced colitis, while ENB was shown to
16 protect mice against various NLRP3-dependent inflammatory conditions [Chen et al., 2019;
17 Jin et al., 2023]. Thus, there is considerable prior functional and preclinical *in vivo* evidence
18 supporting the use of ENB to treat IBD. In here, we show that CD risk variants increase NEK7
19 transcript levels in circulating naïve B cells, with very strong support for “colocalization”
20 ($\theta_{IBD}=0.94$). We also show that expression levels of *NEK7* are affected in multiple circulating
21 immune populations of active CD patients, and – using the data from Kong *et al.*, [2023] – are
22 increased in the colonic epithelium of IBD patients. In addition to supporting a contribution
23 of *NEK7* expression levels in influencing predisposition to IBD, this supports NEK7's role in the
24 disease process *per se*, and hence a more likely curative effect of ENB. We note, however,
25 that the IBD risk variants appears to decrease *NEK7* expression in some gut-resident cells of
26 healthy individuals, while *NEK7* expression is decreased in some circulating immune
27 populations, and these findings deserve further scrutiny.

28 We further identify at least two instances, amongst the targets with approved drugs, where
29 IBD risk variants, rather counterintuitively, increase the expression levels of what are assumed
30 to be positive mediators of inflammation, in particular *IL18R1* and *IL18RAP* on the one hand,
31 and *PTGIR* on the other (Supplemental material). Thus, “hypomorphic” IL18 and prostacyclin
32 pathways may increase the risk to develop IBD, despite the fact that these pathways

1 participate actively in the inflammatory process once initiated. These observations obviously
2 call for caution when intending to use activators of the corresponding pathways to treat active
3 IBD patients. It suggests, however, that treatment of IBD patients in active phase versus
4 relapse should be differentiated. It is conceivable that activation of the IL18 and prostacyclin
5 pathways might help to prevent relapse, particularly after disease remission has been
6 achieved following surgery.

7 Possibly the most important outcome from this work is the suggestion that the notion of
8 polygenicity extends *within* risk loci, and that causative genes in risk loci may influence disease
9 through their effects on multiple cell types. It supports the notion that the genetic
10 determinism of CCD is “quasi-infinitesimal”. This raises the question as to whether targeting
11 individual components of this genetic architecture to treat the disease is the most effective
12 strategy. As mentioned before, it seems unlikely that the effect of the many underpinning
13 risk variants on disease are independent. They must perturb a series of pathways that
14 progressively converge into a limited number of “highways”, that ultimately determine
15 disease outcome. Such “highways” would involve the “core genes” as defined in the
16 omnigenic model [Boyle *et al.*, 2017]. It should, in theory, be possible to genetically
17 reconstruct the topology of the corresponding network. Indeed, just as the disease is
18 associated with multiple risk loci (multiple DAP) “in *trans*”, components of the upper part of
19 the network (the “highways”) are also expected to be associated with multiple risk loci as
20 *trans*-QTL. On the other hand, components of the lower parts of the tree will be associated
21 with fewer risk loci, and ultimately, i.e., at the bottom of the network, only with one (for at
22 least some, as a *cis*-eQTL). It seems that the components of the upper parts of the network
23 (i.e., the “highways”) would make for better drug targets than those at the bottom of the
24 tree. Of note, the abundance of the components of the upper part of the network are
25 expected to be most strongly correlated with polygenic risk scores for the corresponding
26 disease and – if conveniently measurable - may constitute biomarkers capturing both genetic
27 and environmental effects.

28

29 **References**

30 Abdelloui A, Yengo L, Verweij KJH, Visscher PM. 15 years of GWAS discovery: realizing the promise. *Am J Hum*
31 *Genet* **110**: 179-194 (2023).

- 1 Al-Rashed F, Ahmad Z, Thomas R, Melhem M, Snider AJ, Obeid LM, Al-Mulla F, Hannun YA, Ahmad R. Neutral
2 sphingomyelinase 2 regulates inflammatory responses in monocytes/macrophages induced by TNF- α . *Sci Rep*
3 **10**:16802 (2020). doi: 10.1038/s41598-020-73912-5.
- 4 Belinky F, Nativ N, Stelzer G, Zimmerman S, Iny Stein T, Safran M, Lancet D. PathCards: multi-source
5 consolidation of human biological pathways. *Database* **2015**: bav006 (2015). doi:10.1093/database/bav006.
- 6 Bosa L, Batura V, Colavito D, Fiedler K, Gaio P, Guo C, Li Q, Marzollo A, Mescoli C, Nambu R, Pan J, Perilongo G,
7 Warner N, Zhang S, Kotlarz D, Klein C, Snapper SB, Walters TD, Leon A, Griffiths AM, Cananzi M, Muise AM. Novel
8 CARMIL2 loss-of-function variants are associated with pediatric inflammatory bowel disease. *Sci Rep* **11**:5945
9 (2021). doi: 10.1038/s41598-021-85399-9.
- 10 Boyle EA, Li YI, Pritchard JK. An Expanded View of Complex Traits: From Polygenic to Omnigenic. *Cell* **169**:1177-
11 1186 (2017). doi: 10.1016/j.cell.2017.05.038.
- 12 Burclaff J, Bliton RJ, Breau KA, Ok MT, Gomez-Martinez I, Ranek JS, Bhatt AP, Purvis JE, Woosley JT, Magness ST.
13 A proximal-to-distal survey of healthy adult human small intestine and colon epithelium by single-cell
14 transcriptomics. *Cell Mol Gastroenterol Hepatol* **13**:1554–1589 (2022) <https://doi.org/10.1016/j.jcmgh.2022.02.007>
- 15
16 Burgess S, Mason AM, Grant AJ, Slob EAW, Gkatzionis A, Zuber V, Patel A, Tian H, Liu C, Haynes WG, Hovingh GK,
17 Knudsen LB, Whittaker JC, Gill D. Using genetic association data to guide drug discovery and development:
18 review of methods and applications. *Am J Hum Genet* **110**: 195-214 (2023).
- 19 Busse R, et al. Tackling chronic disease in Europe: strategies, interventions and challenges. *European Observatory*
20 *on Health Systems and Policies. Observatory Studies Series n°20* (2010).
- 21 Chen X, Liu G, Yuan Y, Wu G, Wang S, Yuan L. NEK7 interacts with NLRP3 to modulate the pyroptosis in
22 inflammatory bowel disease via NF- κ B signaling. *Cell Death Dis* **10**:906 (2019). doi: 10.1038/s41419-019-2157-1.
- 23 Connally NJ, Nazeen S, Lee D, Shi H, Stamatoyannopoulos J, Chun S, Cotsapas C, Cassa CA, Sunyaev SR. The
24 missing link between genetic association and regulatory function. *eLife* **11**: e74970 (2022).
25 <https://doi.org/10.7554/eLife.74970>
- 26 Delaneau O, Ongen H, Brown AA, Fort A, Panousis NI, Dermitzakis ET. A complete tool set for molecular QTL
27 discovery and analysis. *Nat Commun* **8**: 15452 (2017). <https://doi.org/10.1038/ncomms15452>.
- 28 de Lange K, Moutsianas L, Lee J, Lamb CA, Luo Y, Kennedy NA, Jostins L, Rice DL, Guttierrez-Achury J, Ji S-G, Heap
29 G, Nimmo ER, Edwards C, Henderson P, Mowat C, Sanderson J, Satsangi J, Simmons A, Wilson DC, Tremelling M,
30 Hart A, Mathew CG, Newman WG, Parkes M, Lees CW, Uhlig H, Hawkey C, Prescott NJ, Ahmad T, Mansfield JC,
31 Anderson CA, Barrett JC. Genome-wide association study implicates immune activation of multiple integrin
32 genes in inflammatory bowel disease. *Nat Genet* **49**: 256–261 (2017). <https://doi.org/10.1038/ng.3760>.
- 33 Dimitrov G, Bamberger S, Navard C, Dreux S, Badens C, Bourgeois P, Buffat C, Hugot JP, Fabre A. Congenital
34 Sodium Diarrhea by mutation of the SLC9A3 gene. *Eur J Med Genet.* **262**:103712 (2019). doi:
35 10.1016/j.ejmg.2019.103712.
- 36 Eldjarn GH, Ferkingstad E, Lund SH, Helgason H, Magnusson OT, Gunnarsdottir K, Olafsdottir TA, Halldorsson BV,
37 Olason PI, Zink F, Gudjonsson SA, Sveinbjornsson G, Magnusson MI, Helgason A, Oddsson A, Halldorsson GH,
38 Magnusson MK, Saevardottir S, Eiriksdottir T, Masson G, Stefansson H, Jonsdottir I, Holm H, Rafnar T, Melsted
39 P, Saemundsdottir J, Norddahl GL, Thorleifsson G, Ulfarsson MO, Gudbjartsson DF, Thorsteinsdottir U, Sulem P,
40 Stefansson K. Large-scale plasma proteomics comparisons through genetics and disease associations. *Nature*
41 **622**:348-358 (2023). doi: 10.1038/s41586-023-06563-x.
- 42 Flannick J, Mercader JM, Fuchsberger C, Udler MS, Mahajan A, Wessel J, Teslovich TM, Caulkins L, Koesterer R,
43 Barajas-Olmos F, Blackwell TW, Boerwinkle E, Brody JA, Centeno-Cruz F, Chen L, Chen S, Contreras-Cubas C,
44 Córdova E, Correa A, Cortes M, DeFronzo RA, Dolan L, Drews KL, Elliott A, Floyd JS, Gabriel S, Garay-Sevilla ME,
45 García-Ortiz H, Gross M, Han S, Heard-Costa NL, Jackson AU, Jørgensen ME, Kang HM, Kelsey M, Kim BJ, Koistinen
46 HA, Kuusisto J, Leader JB, Linneberg A, Liu CT, Liu J, Lyssenko V, Manning AK, Marcketta A, Malacara-Hernandez
47 JM, Martínez-Hernández A, Matsuo K, Mayer-Davis E, Mendoza-Caamal E, Mohlke KL, Morrison AC, Ndungu A,
48 Ng MCY, O'Dushlaine C, Payne AJ, Pihoker C; Broad Genomics Platform; Post WS, Preuss M, Psaty BM, Vasan RS,
49 Rayner NW, Reiner AP, Revilla-Monsalve C, Robertson NR, Santoro N, Schurmann C, So WY, Soberón X,
50 Stringham HM, Strom TM, Tam CHT, Thameem F, Tomlinson B, Torres JM, Tracy RP, van Dam RM, Vujkovic M,
51 Wang S, Welch RP, Witte DR, Wong TY, Atzmon G, Barzilai N, Blangero J, Bonnycastle LL, Bowden DW, Chambers
52 JC, Chan E, Cheng CY, Cho YS, Collins FS, de Vries PS, Duggirala R, Glaser B, Gonzalez C, Gonzalez ME, Groop L,

- 1 Kooner JS, Kwak SH, Laakso M, Lehman DM, Nilsson P, Spector TD, Tai ES, Tuomi T, Tuomilehto J, Wilson JG,
2 Aguilar-Salinas CA, Bottinger E, Burke B, Carey DJ, Chan JCN, Dupuis J, Frossard P, Heckbert SR, Hwang MY, Kim
3 YJ, Kirchner HL, Lee JY, Lee J, Loos RJF, Ma RCW, Morris AD, O'Donnell CJ, Palmer CNA, Pankow J, Park KS,
4 Rasheed A, Saleheen D, Sim X, Small KS, Teo YY, Haiman C, Hanis CL, Henderson BE, Orozco L, Tusié-Luna T,
5 Dewey FE, Baras A, Gieger C, Meitinger T, Strauch K, Lange L, Grarup N, Hansen T, Pedersen O, Zeitler P, Dabelea
6 D, Abecasis G, Bell GI, Cox NJ, Seielstad M, Sladek R, Meigs JB, Rich SS, Rotter JI; DiscovEHR Collaboration;
7 CHARGE; LuCamp; ProDiGY; GoT2D; ESP; SIGMA-T2D; T2D-GENES; AMP-T2D-GENES; Altshuler D, Burt NP, Scott
8 LJ, Morris AP, Florez JC, McCarthy MI, Boehnke M. Exome sequencing of 20,791 cases of type 2 diabetes and
9 24,440 controls. *Nature* **570**:71-76 (2019). doi: 10.1038/s41586-019-1231-2.
- 10 Franzén O, Gan L-M, Björkegren JLM. PanglaoDB: a web server for exploration of mouse and human single-cell
11 RNA sequencing data. *Database* 2019: baz046 (2019) <https://doi.org/10.1093/database/baz046>
- 12 Giambertolomei C, Vikcevic D, Schadt EE, Franke L, Hingorani AD, Wallace C, Plagnol V. Bayesian test for
13 colocalization between pairs of genetic association studies using summary statistics. *PLoS Genet* **10**: e1004383
14 (2014).
- 15 GTEx Consortium. The GTEx Consortium atlas of genetic regulatory effects across human tissues. *Science* **369**:
16 1318-1330 (2020).
- 17 Hallows KR, Kobinger GP, Wilson JM, Witters LA, Foskett JK. Physiological modulation of CFTR activity by AMP-
18 activated protein kinase in polarized T84 cells. *Am J Physiol Cell Physiol* **284**:C1297-308 (2003). doi:
19 10.1152/ajpcell.00227.2002.
- 20 Hamaoui D, Subtil A. ATG16L1 functions in cell homeostasis beyond autophagy. *FEBS J* **289**: 1779-1800 (2022).
21 <https://doi.org/10.1111/febs.15833>
- 22 Hao Y, Hao S, Andersen-Nissen E, Mauck WM 3rd, Zheng S, Butler A, Lee MJ, Wilk AJ, Darby C, Zager M, Hoffman
23 P, Stoeckius M, Papalexi E, Mimitou EP, Jain J, Srivastava A, Stuart T, Fleming LM, Yeung B, Rogers AJ, McElrath
24 JM, Blish CA, Gottardo R, Smibert P, Satija R. Integrated analysis of multimodal single-cell data. *Cell* **184**:3573-
25 3587.e29 (2021). doi: 10.1016/j.cell.2021.04.048.
- 26 Hickey JW, Becker WR, Nevins SA, et al. Organization of the human intestine at single-cell
27 resolution. *Nature* **619**: 572–584 (2023). <https://doi.org/10.1038/s41586-023-05915-x>
- 28 Hugot JP, Chamaillard M, Zouali H et al. Association of NOD2 leucine-rich repeat variants with susceptibility to
29 Crohn's disease. *Nature* **411**: 599–603 (2001). <https://doi.org/10.1038/35079107>
- 30 Hormozdiari F, van de Bunt M, Segrè AV, Li X, Joo JWJ, Bilow M, Sul JH, Sankararaman S, Pasaniuc B, Eskin E.
31 Colocalization of GWAS and eQTL signals detects target genes. *Am J Hum Genet* **99**: 1245-1260 (2016).
- 32 Ishikawa K, Sugimoto S, Oda M, Fujii M, Takahashi S, Ohta Y, Takano A, Ishimaru K, Matano M, Yoshida K, Hanyu
33 H, Toshimitsu K, Sawada K, Shimokawa M, Saito M, Kawasaki K, Ishii R, Taniguchi K, Imamura T, Kanai T, Sato T.
34 Identification of quiescent LGR5+ stem cells in the human colon. *Gastroenterology* **163**: 1391-1406 (2022).
- 35 Jakab M, et al. Health systems respond to noncommunicable diseases: time for ambition. *Copenhagen: WHO*
36 *regional Office for Europe* (2018).
- 37 Jiang Q, Li M, Li H, Chen L. Entrectinib, a new multi-target inhibitor for cancer therapy. *Biomed Pharmacother*
38 **150**:112974 (2022). doi: 10.1016/j.biopha.2022.112974.
- 39 Jin X, Liu D, Zhou X, Luo X, Huang Q, Huang Y. Entrectinib inhibits NLRP3 inflammasome and inflammatory
40 diseases by directly targeting NEK7. *Cell Rep Med* **4**:101310 (2023). doi: 10.1016/j.xcrm.2023.101310.
- 41 King EA, Davis JW, Degner JF (2019) Are drug targets with genetic support twice as likely to be approved? Revised
42 estimates of the impact of genetic support for drug mechanisms on the probability of drug approval. *PLoS Genet*
43 **15**: e1008489. <https://doi.org/10.1371/journal.pgen.1008489>.
- 44 Kong L, Pokatayev V, Lefkovith A, Carter GT, Creasey EA, Krishna C, Subramanian S, Kochar B, Ashenberg O, Lau
45 H, Ananthakrishnan AN, Graham DB, Deguine J, Xavier RJ. The landscape of immune dysregulation in Crohn's
46 disease revealed through single-cell transcriptomic profiling in the ileum and colon. *Immunity* **56**: 444-458.e5
47 (2023). doi: 10.1016/j.immuni.2023.01.002.
- 48 Korsunsky I, Millard N, Fan J, Slowikowski K, Zhang F, Wei K, Baglaenko Y, Brenner M, Loh P-r, Raychaudhuri S.
49 Fast, sensitive and accurate integration of single-cell data with Harmony. *Nature Methods* **16**: 1289-1296 (2019).
- 50 Krzak M, Alegbe T, Leland Taylor D, Ghouraba M, Strickland M, Satti R, Thompson T, Arestang K, Przybilla
51 MJ, Ramirez-Navarro L, Harris BT, Cheam KAX, Noell G, Leonard S, Petrova V, Jones-Bell C, James KR, Wana

- 1 N, Hu MX, Skelton J, Ostermayer J, Gu Y, Dawson C, Corridoni D, Cotobal Martin C, Parkes M, Iyer V, Jones
2 G-R, McIntyre RE, Raine T, Anderson CA. Single-cell RNA sequencing reveals dysregulated cellular programmes
3 in the inflamed epithelium of Crohn's disease
4 patients. medRxiv 2023.09.06.23295056; <https://doi.org/10.1101/2023.09.06.23295056>.
- 5 Lesage S, Zouali H, Cézard JP, Colombel JF, Belaiche J, Almer S, Tysk C, O'Morain C, Gassull M, Binder V, Finkel Y,
6 Modigliani R, Gower-Rousseau C, Macry J, Merlin F, Chamaillard M, Jannot AS, Thomas G, Hugot JP; EPWG-IBD
7 Group; EPIMAD Group; GETAID Group. CARD15/NOD2 mutational analysis and genotype-phenotype correlation
8 in 612 patients with inflammatory bowel disease. *Am J Hum Genet* **70**:845-57 (2002). doi: 10.1086/339432.
- 9 Li S, Zhuge A, Chen H, Han S, Shen J, Wang K, Xia J, Xia H, Jiang S, Wu Y, Li L. Sedanolid alleviates DSS-induced
10 colitis by modulating the intestinal FXR-SMPD3 pathway in mice. *J Adv Res* S2090-1232(24)00128-0 (2024). doi:
11 10.1016/j.jare.2024.03.026.
- 12 Liu F, Li X, Yue H, Ji J, You M, Ding L, Fan H, Hou Y. TLR-Induced SMPD3 Defects Enhance Inflammatory Response
13 of B Cell and Macrophage in the Pathogenesis of SLE. *Scand J Immunol* **86**:377-388 (2017). doi:
14 10.1111/sji.12611.
- 15 Liu D, Offin M, Harnicar S, Li BT, Drilon A. Entrectinib: an orally available, selective tyrosine kinase inhibitor for
16 the treatment of *NTRK*, *ROS1*, and *ALK* fusion-positive solid tumors. *Ther Clin Risk Manag* **14**:1247-1252 (2018).
17 doi: 10.2147/TCRM.S147381.
- 18 Liu X, Li YI, Pritchard JK. *Trans* effects on gene expression can drive omnigenic inheritance. *Cell* **177**:1022-1034
19 (2019).
- 20 Magg T, Shcherbina A, Arslan D, Desai MM, Wall S, Mitsialis V, Conca R, Unal E, Karacabey N, Mukhina A, Rodina
21 Y, Taur PD, Illig D, Marquardt B, Hollizeck S, Jeske T, Gothe F, Schober T, Rohlf M, Koletzko S, Lurz E, Muise AM,
22 Snapper SB, Hauck F, Klein C, Kotlarz D. CARMIL2 Deficiency Presenting as Very Early Onset Inflammatory Bowel
23 Disease. *Inflamm Bowel Dis* **25**:1788-1795 (2019). doi: 10.1093/ibd/izz103.
- 24 Minikel EV, Painter JL, Dong CC, Nelson MR. Refining the impact of genetic evidence on clinical success. *Nature*
25 **629**:624-629 (2024). doi: 10.1038/s41586-024-07316-0.
- 26 Mohanan V, Nakata T, Desch AN, Lévesque C, Boroughs A, Guzman G, Cao Z, Creasey E, Yao J, Boucher G, Charron
27 G, Bhan AK, Schenone M, Carr SA, Reinecker HC, Daly MJ, Rioux JD, Lassen KG, Xavier RJ. *C1orf106* is a colitis risk
28 gene that regulates stability of epithelial adherens junctions. *Science* **359**:1161-1166 (2018). doi:
29 10.1126/science.aan0814.
- 30 Momozawa Y, Dmitrieva J, Théâtre E, Deffontaine V, Rahmouni S, Charlotheaux B, Crins F, Decampo E, Elansary
31 M, Gori A-S, Lecut C, Mariman R, Mni M, Oury C, Altukhohov I, Alexeev D, Aulchenko Y, Amininejad L, Bouma G,
32 Hoentjen F, Löwenberg F, Oldenburg B, Pierik MJ, vander Meulen-de Joing AE, van der Woude J, Visschedijk MC,
33 The IIBDGC, Lathrop M, Hugot J-P, Weersma RK, De Vos M, Franchimont D, Vermeire S, Kubo M, Louis E, Georges
34 M. IBD risk loci are enriched in multigenic regulatory modules encompassing putative causative genes. *Nat*
35 *Commun* **9**: 2427 (2018). <https://doi.org/10.1038/s41467-018-04365-8>
- 36 Mostafavi H, Spence JP, Naqvi S, Pritchard JK. Systematic differences in discovery of genetic effects on gene
37 expression and complex traits. *Nat Genet* **55**: 1866–1875 (2023). <https://doi.org/10.1038/s41588-023-01529-1>.
- 38 Mountjoy E, Schmidt EM, Carmona M, Schwartzenruber J, Peat G, Miranda A, Fumis L, Hayhurst J, Buniello A,
39 Karim MA, Wright D, Hercules A, Papa E, Fauman EB, Barrett JC, Todd JA, Ochoa D, Dunham I, Ghousaini M. An
40 open approach to systematically prioritize causal variants and genes at all published human GWAS trait-
41 associated loci. *Nat Genet* **53**:1527-1533 (2021). doi: 10.1038/s41588-021-00945-5.
- 42 Ota M, Nagafuchi Y, Hatano H, Ishigaki K, et al. Dynamic landscape of immune cell-specific gene regulation in
43 immune-mediated diseases. *Cell* **184**: 3006-3021.e17 (2021). <https://doi.org/10.1016/j.cell.2021.03.056>.
- 44 Polubriaginof FCG, Vanguri R, Quinnes K, Belbin GM, Yahi A, Salmasian H, Lorberbaum T, Nwankwo V, Li L,
45 Shervey MM, Glowe P, Ionita-Laza I, Simmerling M, Hripcsak G, Bakken S, Goldstein D, Kiryluk K, Kenny EE, Dudley
46 J, Vawdrey DK, Tatonetti NP. Disease heritability inferred from familial relationships reported in medical records.
47 *Cell* **173**: 1692-1704 (2018).
- 48 Prieto S, Dubra G, Camasses A, Aznar AB, Begon_Pescia C, Simboeck E, Pirot N, Gerbe F, Angevin L, Jay P,
49 Krasinska L, Fisher D. CDK8 and CDK19 act redundantly to control the CFTR pathway in the intestinal epithelium.
50 *EMBO rep* **24**: e54261 (2022). <https://doi.org/10.15252/embr.202154261>
- 51 Roncagalli R, Cucchetti M, Jarmuzynski N, Grégoire C, Bergot E, Audebert S, Baudalet E, Menoita MG, Joachim
52 A, Durand S, Suchanek M, Fiore F, Zhang L, Liang Y, Camoin L, Malissen M, Malissen B. The scaffolding function

- 1 of the RLTPR protein explains its essential role for CD28 co-stimulation in mouse and human T cells. *J Exp Med*
2 **213**:2437-2457 (2016). doi: 10.1084/jem.20160579.
- 3 Sazonovs A, Stevens CR, Venkataraman GR *et al.* Large-scale sequencing identifies multiple genes and rare
4 variants associated with Crohn's disease susceptibility. *Nat Genet* **54**: 1275–1283 (2022).
5 <https://doi.org/10.1038/s41588-022-01156-2>.
- 6 Schmiedel BJ, Singh D, Madrigal A, Valdovino-Gonzalez AG, White BM, Zapardiel-Gonzalo J, Ha B, Altay G,
7 Greenbaum JA, McVicker G, Seumoio G, Rao A, Kronenberg M, Peters B, Vijayanand P. impact of genetic
8 polymorphisms on human immune cell gene expression. *Cell* **175**: 1701-1715 (2018).
9 <https://doi.org/10.1016/j.cell.2018.10.022>
- 10 Schumacher A, Gassmann O, Hinder M. Changing R&D models in research-based pharmaceutical companies. *J*
11 *Transl Med* **14**: 105 (2016).
- 12 Smillie CS, Biton M, Ordovas-Montanes J, Sullivan KM, Burgin G, Graham DB, Herbst RH, Rogel N, Slyper M,
13 Waldman J, Sud M, Andrews E, Velonias G, Haber AL, Jagadeesh K, Vickovic S, Yao J, Stevens C, Dionne D, Nguyen
14 LT, Villani AC, Hofree M, Creasey EA, Huang H, Rozenblatt-Rosen O, Garber JJ, Khalili H, Desch AN, Daly MJ,
15 Ananthakrishnan AN, Shalek AK, Xavier RJ, Regev A. Intra- and Inter-cellular Rewiring of the Human Colon during
16 Ulcerative Colitis. *Cell* **178**: 714-730.e22 (2019). doi: 10.1016/j.cell.2019.06.029.
- 17 Stegle O, Parts L, Durbin R, Winn J. A Bayesian framework to account for complex non-genetic factors in gene
18 expression levels greatly increases power in eQTL studies. *PLoS Comput Biol* **6**: e1000770 (2010).
19 <https://doi.org/10.1371/journal.pcbi.1000770>.
- 20 Steinmetz L, Sinha H, Richards D, Spigelman JI, Oefner PJ, McCusker JH, Davis RW. Dissecting the architecture of
21 a quantitative trait locus in yeast. *Nature* **416**: 326–330 (2002). <https://doi.org/10.1038/416326a>
- 22 Stern DL. Identification of loci that cause phenotypic variation in diverse species with the reciprocal hemizyosity
23 test. *Trends Genet* **30**:547-554 (2014). doi: 10.1016/j.tig.2014.09.006.
- 24 Storey JD, Tibshirani R. Statistical significance for genomewide studies. *Proc Natl Acad Sci USA* **100**:9440-9445
25 (2003). doi: 10.1073/pnas.1530509100.
- 26 Taniguchi K, Inoue M, Arai K, Uchida K, Migita O, Akemoto Y, Hirayama J, Takeuchi I, Shimizu H, Hata K. Novel
27 TNFAIP3 microdeletion in a girl with infantile-onset inflammatory bowel disease complicated by a severe
28 perianal lesion. *Hum Genome Var* **8**:1 (2021). doi: 10.1038/s41439-020-00128-4.
- 29 The International HapMap Consortium. A haplotype map of the human genome. *Nature* **437**: 1299-1320 (2005).
- 30 Thurman RE, Rynes E, Humbert R, Vierstra J, Maurano MT, Haugen E, Sheffield NC, Stergachis AB, Wang H,
31 Vernet B, Garg K, John S, Sandstrom R, Bates D, Boatman L, Canfield TK, Diegel M, Dunn D, Ebersol AK, Frum T,
32 Giste E, Johnson AK, Johnson EM, Kutayavin T, Lajoie B, Lee BK, Lee K, London D, Lotakis D, Neph S, Neri F, Nguyen
33 ED, Qu H, Reynolds AP, Roach V, Safi A, Sanchez ME, Sanyal A, Shafer A, Simon JM, Song L, Vong S, Weaver M,
34 Yan Y, Zhang Z, Zhang Z, Lenhard B, Tewari M, Dorschner MO, Hansen RS, Navas PA, Stamatoyannopoulos G,
35 Iyer VR, Lieb JD, Sunyaev SR, Akey JM, Sabo PJ, Kaul R, Furey TS, Dekker J, Crawford GE, Stamatoyannopoulos JA.
36 The accessible chromatin landscape of the human genome. *Nature* **489**:75-82 (2012). doi: 10.1038/nature11232.
- 37 Trajanoska K, Bhérer C, Taliun D, Zhou S, Richards JB, Mooser V. From target discovery to clinical drug
38 development with human genetics. *Nature* **620**:737-745 (2023). doi: 10.1038/s41586-023-06388-8.
- 39 Umans BD, Battle A, Gilad Y. Where are the disease-associated eQTLs? *Trends Genet* **37**: 109-124 (2021).
- 40 Vieujean S, Jairath V, Peyrin-Biroulet L, Dubinsky M, Iacucci M, Magro F, Danese S. understanding the therapeutic
41 toolkit for inflammatory bowel disease. *Nat Rev Gastroenterol Hepatol*, in the press (2024).
- 42 Visscher, PM, Wary NR, Zhang Q, Sklar P, McCarthy MI, Brown MA, Yang J. 10 Years of GWAS discovery: biology,
43 function, and translation. *Am J Hum Genet* **101**: 5-22 (2017).
- 44 Vösa U, Claringbould A, Westra HJ. *et al.* Large-scale *cis*- and *trans*-eQTL analyses identify thousands of genetic
45 loci and polygenic scores that regulate blood gene expression. *Nat Genet* **53**: 1300–1310 (2021).
46 <https://doi.org/10.1038/s41588-021-00913-z>.
- 47 Watanabe K, Stringer S, Frei O, Mirkov MU, de Leeuw C, Polderman TJC, van der Sluis S, Andreassen OA, Neal
48 BM, Posthuma D. A global overview of pleiotropy and genetic architecture in complex traits. *Nat Genet* **51**: 1339-
49 1348 (2019).

- 1 Yan J, Hedl M, Abraham C. An inflammatory bowel disease-risk variant in INAVA decreases pattern recognition
2 receptor-induced outcomes. *J Clin Invest* **127**:2192-2205 (2017). doi: 10.1172/JCI86282.
- 3 Yıldız Ç, Gezgin Yıldırım D, İnci A, Tümer L, Cengiz Ergin FB, Sunar Yayla ENS, Esmeray Şenol P, Karaçayır N, Eğritaş
4 Gürkan Ö, Okur I, Ezgü FS, Bakkaloğlu SA. A possibly new autoinflammatory disease due to compound
5 heterozygous phosphomevalonate kinase gene mutation. *Joint Bone Spine* **90**:105490 (2023). doi:
6 10.1016/j.jbspin.2022.105490.
- 7 Yu M, Zhang Q, Yuan K, Sazonovs A, Stevens C, IBDGC, Anderson CA, Daly MJ, Huang H. Cystic fibrosis risk
8 variants confer protective effects against inflammatory bowel disease in large-scale exome sequencing analysis.
- 9 Zhu, Z., Zhang, F., Hu, H. *et al.* Integration of summary data from GWAS and eQTL studies predicts complex trait
10 gene targets. *Nat Genet* **48**: 481–487 (2016). <https://doi.org/10.1038/ng.3538>.
- 11 Zou D, Zhou S, Wang H, Gou J, Wang S. Knee Joint Swelling at Presentation: A Case of Pediatric Crohn Disease
12 With a TNFAIP3 Mutation. *Pediatrics* **146**:e20193416 (2020). doi: 10.1542/peds.2019-3416.

13

14

15 **Methods**

16 ***Identifying cis-eQTL modules in bulk RNA-Seq data of 27 sorted circulating immune cell*** 17 ***populations.***

18 **Sample collection.** We collected 40 ml of venous blood (EDTA) from 251 healthy European
19 subjects at the academic hospital of the University of Liège (CHU) between October 2018 and
20 November 2022. Written informed consent was obtained prior to donation in agreement
21 with the recommendations of the declaration of Helsinki for experiments involving human
22 subjects. The experimental protocol was approved by the Ethics committee of the CHU Liège
23 (reference number: 2017/214). Data collected from the electronic medical records (EMR)
24 included birth date, age at sampling, ancestry, sex, weight, height, smoking and alcohol
25 history, declared ethnicity, family history of disease, surgical and medication history, blood
26 type when available and known allergies. The following hematological parameters were
27 measured: counts of white blood cells, neutrophils, lymphocytes, monocytes, eosinophils,
28 basophils, platelets, red blood cells, hemoglobin concentration, hematocrit, mean cell
29 volume, mean cell hemoglobin, mean cell hemoglobin concentration, red cell distribution
30 width and mean platelet volume (STable 1).

31 **SNP genotyping.** Genomic DNA was isolated from frozen EDTA-blood using the NucleoMag
32 Blood 200 µL kit (Macherey-Nagel) on a KingFisher robot (Thermo Fisher Scientific).
33 Individuals were genotyped for 713,606 SNPs using Illumina's Human OmniExpress
34 BeadChips, an iScan system and the Genome Studio software following the guidelines of the
35 manufacturer. We confirmed the European ancestry of the participants by PCA (using the
36 HapMap population as reference) as well as the absence of duplicated or related individuals

1 (pi hat > 0.185). All individuals had less than 3% of missing genotypes. We excluded variants
2 with call rate ≤ 0.95 or deviating from Hardy–Weinberg equilibrium ($p \leq 3 \times 10^{-4}$) using plink
3 (v1.9), leaving 689,223 quality-controlled variants. After lifting over to GRCh38 using Picard
4 LifterVcf (v2.7.1), we phased and imputed to whole genome using the TOPMed Imputation
5 Server (v1.6.6) and the TOPMed r2 reference panel. We removed variants with imputation
6 score (R^2) ≤ 0.7 or minor allele frequency (MAF) ≤ 0.05 using bcftools (v1.11), leaving
7 genotypes at 6,299,998 QC-ed variants.

8 **Cell sorting.** Granulocytes were isolated from blood using the EasySep™ Direct Human Pan-
9 Granulocyte Isolation Kit (StemCell Technologies #19659) within one hour after collection.
10 Neutrophils and eosinophils were then isolated from the recovered granulocytes using the
11 EasySep™ Human Neutrophil Isolation Kit (StemCell Technologies #17957) and EasySep™
12 Human Eosinophil Isolation Kit (StemCell Technologies #17956), respectively. Cells were
13 recovered in cell homogenization buffer provided with the Maxwell 16 LEV simply RNA Tissue
14 Kit (Promega #AS1280) or the AllPrep DNA/RNA Micro Kit (Qiagen #80284), and immediately
15 frozen at -80°C until use.

16 Peripheral blood mononuclear cells (PBMC) were isolated from fresh blood using SepMate™-
17 50 (IVD) collection tubes (StemCell Technologies #85460) and Lymphoprep™ density gradient
18 medium (StemCell Technologies #07861). After two washing steps, PBMC were stained with
19 two panels of antibodies for 30 minutes at 4°C (STable 28). Cells suspended in PBS were then
20 filtered using a $100\ \mu\text{m}$ CellTrics filter (Sysmex #04004-2328). Cell sorting was performed on
21 a FACS Aria III instrument (BD Biosciences) calibrated using CS&T beads (BD Biosciences).
22 Fluorescence compensations were performed using CompBeads (BD Biosciences #552843).
23 After exclusion of debris and doublets, we targeted monocytes (classical, non-classical and
24 intermediate), T lymphocytes (including $\gamma\delta$, mucosal-associated invariant T cells (MAIT) cells,
25 naive and memory regulatory T cells, naive and memory CD8+ T cells, naive and memory CD4+
26 T cells, Th1, Th2, Th17 and Th1/17 helper T cells), B lymphocytes (naive, memory and
27 plasmacytes), dendritic cells (plasmacytoid and myeloid), natural killer cells (NK and NKT) and
28 innate lymphoid cells (ILC). Panels of antibodies used, definition of sorted cells and gating
29 strategies are described in SFig. 1 and STable 28. Purity of the sorted cell populations ranged
30 from 78% to 99%. Up to 20,000 cells of each cell population were sorted directly on the cell
31 homogenization buffer and frozen immediately at -80°C until use.

1 **Bulk RNA sequencing.** Total RNA was purified from sorted cells using the Maxwell 16 LEV
2 simplyRNA Tissue Kit (Promega #AS1280) on a Maxwell 16 instrument (Promega) or manually
3 using the AllPrep DNA/RNA Micro Kit (Qiagen #80284) with the QIAshredder (Qiagen #79656),
4 according to their respective manufacturer's instructions. RNA quantity was determined for
5 all samples using the Quant-iT RiboGreen RNA Assay Kit (ThermoFisher Scientific #R11490),
6 while the RNA quality has been evaluated for a subset of samples using the RNA 6000 Pico Kit
7 on a 2100 Bioanalyzer instrument (Agilent #5067-1513). Reagents for cDNA and library
8 preparation were dispensed with a Mantis Liquid Handler (Formulatrix) using half the
9 recommended volumes. Full-length cDNA was generated from 1 ng of total RNA using the
10 SMART-Seq HT Kit (Takara #634436), which poly-A selects mRNAs. Obtained cDNA quantity
11 and quality were determined for all samples using the Quant-iT PicoGreen dsDNA Assay Kit
12 (ThermoFisher Scientific #P7589), and for some using the High Sensitivity DNA kit on a 2100
13 Bioanalyzer instrument (Agilent #5067-4626), respectively. Uniquely indexed libraries were
14 constructed from 300 pg of cDNA using the Nextera XT DNA Library Preparation Kit (Illumina
15 #FC-131-1096) and custom-made 24 forward and 16 reverse primers. The libraries' quantity
16 was assessed for all samples by qPCR using a KAPA Library Quantification Kit
17 (Roche#07960140001), while the libraries' quality was checked for all samples using a QIAxcel
18 Advanced technology (Qiagen). The libraries were pooled and sequenced on a NovaSeq 6000
19 instrument (Illumina), to an average read depth of 11 ± 5 million paired-end reads per sample
20 (University of Geneva core facility (Geneva): 2x50 bp (2,112 samples); GIGA Genomics
21 platform (Liège): 2x150 bp (3,180 samples)). We performed RNA-seq for 5,292 samples,
22 corresponding to 27 cell types from 196 individuals.

23 **Read mapping and quantification.** Demultiplexing and FASTQ conversion were performed
24 using bcl2fastq (v2.20). Read quality was assessed with FastQC (v0.12.1) and multiQC (v0.9).
25 Reads were mapped to the GRCh38 (Ensembl release 105) human genome build using STAR
26 (v2.7.1a). The STAR re-implementation of the WASP algorithm was used with a custom VCF
27 file containing both reference and alternative alleles for all SNPs. The alignments that did not
28 pass WASP filtering or that overlapped indels were removed from the resulting BAM files
29 using samtools (v1.9). Alignment metrics were collected using Picard CollectRnaSeqMetrics
30 (v2.7.1) (STable 3). Matching of genomic and transcriptome genotypes was evaluated with
31 QTLtools mbv (v1.3.1) (SFig. 2A). Unstranded gene counts were generated with HTSeq
32 (v0.6.1p1). If samples were split across two sequencing lanes, we summed up the respective

1 counts. To detect mislabeled samples, reads counts were normalized using the variance
2 stabilizing transformation from the DESeq2 R package and a t-SNE analysis was conducted
3 using the 500 most variable genes (SFig. 2). STable 3 reports the characteristics of the 5,030
4 RNA-seq libraries that passed the quality control procedure.

5 **Transcriptome-based hierarchical clustering of circulating immune cell types.** A dendrogram
6 was constructed based on the RNA-seq data, using $1 - |\text{Spearman's correlation}|$ between
7 average (across all individuals) gene expression levels, using the “average”, “ward.d” and
8 “ward.d2” methods. For each method, we built 32 dendrograms with from 250 to 8000 (by
9 steps of 250) genes with best F statistic (cell type effect) from ANOVA. Within each method,
10 we assessed the reliability of each dendrogram in a way inspired by the bootstrap procedure:
11 for each node in the dendrogram, we computed the proportion among the 31 other trees
12 that shared the same split. Within each method, we selected the dendrogram(s) with the
13 highest sum of “bootstrap-like” values. Memory CD4 T cells, PBMC and granulocytes were
14 ignored in this analysis as they encompass multiple cell types.

15 **Cis-eQTL analyses.** For each blood cell type, we filtered out the genes with less than 5 counts
16 in more than 80% of samples, normalized the raw read counts using the DESeq2 R package
17 and residualized them for age, sex, RNA extraction method, proportion of reads in each
18 sequencing batch, top 3 genotype principal components (PCs) and top 13-36 expression PCs
19 to maximize the number of *cis*-eQTLs. STable 4 reports the number of samples, genes and top
20 expression PCs for each cell type. We removed variants with $\text{MAF} \leq 0.05$ in the retained
21 samples using bcftools (v1.9) for each cell type. We performed eQTL mapping using QTLtools
22 in a 2 Mb window centered at the transcription start site and with the integrated rank normal
23 transformation of the phenotypes. The *p*-values were corrected for multiple testing within
24 each window by permutation (10,000 permutations) and within each cell type using the false
25 discovery rate (FDR). eQTL with “within cell type FDR” ≤ 0.05 were considered significant.

26 **Proportion of expression variance explained by *cis*-eQTLs.** The proportion of expression
27 variance was computed as $2pq\beta^2$, where *p* and *q* are the allelic frequencies of reference and
28 alternate allele, respectively, and β is the slope of the regression line of standardized gene
29 expression (mean: 0, variance: 1) on dosage of the alternate allele, i.e., the allele substitution
30 effect. This gave near identical results as QTLtools (r-squared values).

31 **Agglomerating *cis*-eQTL in gene-specific and across-genes *cis*-acting regulatory modules**
32 **(RM).** To assess if the expression levels of a given gene are affected by the same regulatory

1 variants in a given pair of tissues, we compared the corresponding eQTL association patterns
2 (EAP) using the θ metric devised in Momozawa *et al.* [2018]. Two EAP were compared if at
3 least one of them was significant ($FDR \leq 0.05$). We only used variants that had a p -value
4 below 0.05 in at least one of the two EAP to compute θ . Two EAP were assumed to be part
5 of the same *cis*-acting regulatory module (RM) if $|\theta| \geq 0.6$ (cfr. Momozawa *et al.* [2018]), and
6 if the window-adjusted p -value of the eQTL (for non-significant eQTL) was ≤ 0.12 , as these
7 parameter values were shown to yield an agglomeration $FDR \leq 0.05$ in a permutation test
8 (see DAP-EAP matching section, hereafter). To better describe the connectivity of the
9 modules, we retrospectively also computed θ for pairs of non-significant EAP if they were
10 assigned to the same module. We first constructed gene-specific modules, i.e., we only
11 confronted EAP from the same gene yet from different cell types. In a second stage, we
12 constructed across-gene modules by evaluating the similarity of the EAP of different genes in
13 the same or in different tissues, using the union of the overlapping 2 Mb windows, and using
14 the same threshold values as above. We defined a representative EAP for each module as
15 the EAP with the lowest adjusted p -value for β . For all EAP in a module, the sign of β was
16 compared to that of the representative EAP. If the modules encompassed more than one
17 EAP, we performed a meta-analysis to combine the constituent EAP in a consensus EAP
18 representing the module. For each variant of the complete window (2-4 Mb), we converted
19 nominal p -values to z -score which we squared and summed across all EAP in the module.
20 The corresponding sum was assumed to have a chi-squared distribution with degrees of
21 freedom equal to the number of EAP in the module. When arithmetic underflow was reached
22 for the p -values, the $-\log_{10}(p)$ values were predicted from the z -scores using a local
23 polynomial regression. RMs were then curated to remove the connections between non-
24 similar EAP. The similarity between the EAP and their consensus EAP was assessed using θ .
25 If $|\theta| < 0.6$, the EAP were excluded from the module and the consensus EAP reconstructed.
26 Similarity between excluded EAP was tested to allow them to form distinct “sub-RM”.

27 **Quantifying the statistical significance of the overdispersion of module activity across cell**
28 **types.** We quantified the dispersion for the real data, as the variance of the sum of active cell
29 types across modules. We then performed “permutations”, in the sense that – for a given
30 cell type – the activity states (1’s and 0’s) were permuted between modules. This was
31 repeated for all cell types, and the dispersion of that permutation computed as the variance
32 of the sum of “active” cell types across modules. The statistical significance of the real

1 dispersion was then defined as the proportion of permutations that yielded as large or larger
2 variance than the real data.

3 **Assigning modules to nodes and leaves in the ontogenic dendrogram.** Gene-specific
4 modules were assigned to nodes and leaves of the best supported ontogenic tree (SFig. 2C).
5 Modules that encompassed only one cell type were assigned to the leaves of the tree while
6 modules that encompassed more than one cell type were assigned to the node corresponding
7 to the most recent common ancestor (MRCA) of those cell types. Descendants of such MRCA
8 nodes that were not encompassed by the module were assumed to have lost the eQTL effect.
9 If these were part of another regulatory module for the same gene, the “loss” was converted
10 to a “switch”. Memory CD4 T cells, PBMC and granulocytes were ignored in this analysis (cfr.
11 above).

12 **Testing for an excess sharing of RM between cell types.** We followed Momozawa *et al.*
13 [2018] to test whether specific cell types were sharing *cis*-eQTL more often than expected by
14 chance (expected for ontogenically related cell types). In our analysis framework, this would
15 manifest itself by the fact that the corresponding cell types would be co-included in the same
16 RM more often than expected by chance. The number of *cis*-eQTL detected by cell type
17 differs, and this has to be taken into account when measuring enrichment. We assumed that
18 if sharing of eQTL was equally likely for any pair of cell types (accounting for differing numbers
19 of eQTL per cell type), the proportion of sharing events between cell type i and j should
20 correspond to the proportion of eQTL detected in cell type j (n_{jT}) out of all eQTL detected in
21 all cell types other than i ($\sum_{k \neq i}^{27} n_{kT}$). Imagine that cell type i is characterized by a total of
22 n_{iS} sharing events, where $n_{iS} = \sum_{k \neq i}^{27} n_{ik}$, and n_{ik} is the observed number of sharing
23 events between cell type i and k . We determined the probability to obtain n_{ij} or more
24 “successes” under the null, by sampling n_{iS} events with a probability of success of $\frac{n_{jT}}{\sum_{k \neq i}^{27} n_{kT}}$
25 by simulation ($n = 5,000$). Of note, this process yields two p -values for every pair i, j : one
26 obtained when considering i as reference, the other when considering j as reference. As in
27 Momozawa *et al.*, we performed the analysis 26 times: first considering RM with no more
28 than two cell-types (hence eQTL that are shared by two cell types only), then considering RM
29 with no more than three cell-types, etc., until considering RM encompassing all cell types.

30 **Probing the causes of the cell type-specificity of gene-specific RM.** Why is a *cis*-eQTL for
31 gene “X” detected in cell type a but not b ? We distinguished three possible scenarios: (i)

1 Module switch: gene “X” is subject to a *cis*-eQTL effect in both cell type *a* and *b*, but the
2 variants involved are distinct (i.e. dissimilar EAP), and the two *cis*-eQTL are assigned to
3 different RM, (ii) Lack of expression cell type *b*: gene “X” is expressed at too low levels in cell
4 type *b* to allow for the detection of a *cis*-eQTL effect, and (iii) Conditional eQTL effects: gene
5 “X” is expressed at sufficient levels in cell type *b*, but there is no evidence for a *cis*-eQTL effect
6 (significant variants x cell type interaction effect). To test the statistical significance of the
7 third scenario, we first measured the *cis*-eQTL effect at the top variant for cell type *a*, in cell
8 types *a* and *b*, yielding β_a and β_b . We then generated bootstrap samples from cell type *a*,
9 and computed 1,000 β_s 's. The *p*-value of the variant x cell type interaction was determined
10 as the number of β_s -values that would be equal or lower than β_b if β_a was positive, or equal
11 or higher than β_b if β_a was negative.

12

13 ***Identifying cis-eQTL modules in single-cell RNA-Seq data from intestinal biopsies at three*** 14 ***anatomical locations.***

15 **Sample collection.** Gut biopsies were obtained from 60 healthy adults (27 females and 33
16 males, average age was 54 years ranging from 23 to 75) that were visiting the university
17 hospital of the University of Liège as part of a screening campaign for colon cancer between
18 June 2019 and December 2021. Written informed consent was obtained prior to donation in
19 agreement with the recommendations of the declaration of Helsinki for experiments
20 involving human subjects. The experimental protocol was approved by the Ethics committee
21 of CHU Liège (reference number: 2017/214). Two to four biopsy “bites” were collected from
22 rectum (RE) and transverse colon (TC) for all participants while biopsies from the terminal
23 ileum (IL) were obtained for 52. Biopsies were collected in 40 ml of RPMI-1640 culture
24 medium (Lonza Bioscience, 12-167F) supplemented with 2 mM L-Glutamine (Thermo Fisher
25 Scientific, 25030024) and 10% FBS (Sigma, F7524) on ice, and processed freshly within one
26 hour from the time of colonoscopy. Data collected from the electronic medical record (EMR)
27 were the same as for the individuals providing blood samples (STable 1).

28 **SNP genotyping.** Was conducted using the same procedure as for the circulating immune cell
29 population samples (see above). We kept 686,493 SNPs interrogated by Illumina's
30 OmniExpress array after quality control, while genotypes at 6,352,658 variant positions were
31 kept after imputation and quality control.

1 **Single-cell RNA sequencing.** Biopsies from the three locations (IL, TC, RE) were processed in
2 parallel using so-called two-step protocols [Smillie *et al.*, 2019; Kong *et al.*, 2023] with some
3 modifications. Fractionation of epithelial (EC) and lamina propria (LP) cell layers: The biopsies
4 delivered in the transport media were collected by passing the media through a 100 µm cell
5 strainer (Pluriselect Life Science, 43-50100-50), and transferred to a 50 ml EZFlip tube
6 (Thermo Fisher Scientific, 10571663) with 25 ml of pre-warmed Epithelial Strip Buffer
7 consisting of HBSS (Thermo Fisher Scientific, 14170088), 5 mM EDTA (Thermo Fisher
8 Scientific, AM9260G), 15 mM HEPES (Lonza Bioscience, 17-737E) and 5% FBS and a magnetic
9 stirring bar. The sample was agitated with gentle stirring (130 rpm) for 10 min at 37°C by
10 placing the tube upside down on a magnetic stirrer (Thermo Fisher Scientific, 50088009) in a
11 37°C incubator. After adding DTT to a final concentration of 1 mM (VWR, 443852A), the
12 sample was incubated for another 10 min with agitation at 37°C. The sample was taken out
13 of the incubator and shaken by hand vigorously for 10 – 15 seconds. It was passed through a
14 100 µm cell strainer to fractionate EC in the flow-through in a new 50 ml canonical tube, while
15 the LP remained on the cell strainer. The LP sample on the strainer was rinsed with Washing
16 Buffer (HBSS supplemented with 1 mM EDTA and 1% FBS) and kept on ice in a 6-well
17 containing Wash Buffer. Dissociation of EC: The tube with the EC fraction was filled with ice-
18 cold Washing Buffer up to 50 ml and centrifuged at 500 rcf for 5 min at 4°C. After carefully
19 removing the supernatant, the sample was transferred to a 1.5 ml siliconized microtube
20 (Sigma, T4816) using 100 µl of TrypLE Express enzyme solution (Thermo Fisher Scientific,
21 12604-013). The sample was then mixed ten times using a 200 µl tip and incubated in a water
22 bath at 37°C for 5 min. The reaction was stopped by adding 1 ml of ice-cold Wash Buffer. EC
23 were collected by centrifugation at 500 rcf for 5 min at 4°C, and resuspended in 100 µl of PBS
24 (Lonza Bioscience, 17-516F) with 10% FBS. Cell concentration and viability was estimated by
25 staining 10 µl of cell suspension with an equal volume of 0.4% Trypan blue solution (Lonza
26 Bioscience, 17-942E) using either TC20 (Bio-Rad) or Countess 3 (Thermo Fisher Scientific)
27 automated cell counters. We obtained an average of 4.1E+05, 2.6E+05 and 1.7E+05 EC cells
28 with viability of 58%, 47% and 47% for IL, TC and RE, respectively. Dissociation of LP cells: The
29 LP remaining on the cell strainer was transferred to a gentleMACS C tube (Miltenyi Biotec,
30 130-093-237) using 15 ml of pre-warmed Enzyme Solution consisting of HBSS supplemented
31 with 2.5 mg of Liberase TL (Roche, 05401020001), 7.5 U of DNase I (Thermo Fisher Scientific,
32 EN052) and 2% FBS. The LP tissue was dissociated using a gentleMACS Octo Dissociator

1 (Miltenyi Biotec) with “37C_m_LPDK” program (~ 25 min). Large debris were filtered out by
2 passing the cell suspension through a 100 µm cell strainer into a new 50 ml tube. The tube
3 was filled with ice-cold Washing Buffer up to 50 ml and spun at 500 rcf for 5 min at 4°C. After
4 carefully removing the supernatant, the sample was treated with TrypLE Express enzyme and
5 resuspended in 100 µl of PBS with 10% FBS as described above. We obtained an average
6 $9.1E+05$, $8.6E+05$ and $5.5E+05$ LP cells with viability of 74%, 78% and 77% for IL, TC and RE,
7 respectively. Cell hashing: To reduce technical batch effects and costs of droplet-based
8 scRNA-Seq [Stoeckius *et al.* 2018], we labeled each fraction of cells with distinct oligo-tagged
9 antibodies and performed droplet formation using all fractions from a donor together in a
10 single well of a 10X Genomics Chromium system. As we generally obtained larger numbers of
11 cells from LP than EC, the LP cell suspension was divided into two or three tubes, while EC
12 was kept in one tube (total 10 tubes). The total volume of the cell suspension per tube was
13 adjusted to 90 µl using PBS with 10% FBS. The cell suspensions were first incubated with 5 µl
14 of Human TruStain FcX Fc receptor blocking solution (BioLegend, 422301) for 10 min at 4°C,
15 then mixed with 2 µl of 10 times diluted unique TotalSeq-B anti-human Hashtag antibodies
16 (Biolegend; see also STable 10) and incubated at 4°C for 30 min. The cells were washed twice
17 by adding 1 ml of PBS with 10% FBS and centrifuged at 400 rcf for 5 min at 4°C. The cells were
18 re-suspended in 100 µl of PBS with 10% FBS and cell density and viability was estimated as
19 described above. Equalized numbers of cells (average of 70,000 cells per tube) were pooled
20 into one tube. In addition, 20,000 non-labeled cells were added in the pool, to provide base
21 lines of hashtag reads when demultiplexing sequencing data. The cell pool was washed once
22 more and re-suspended in 100 ~ 400 µl of PBS with 10% FBS. After filtering through a 70 µm
23 filter followed by a 40 µm cell strainer (Thermo Fisher Scientific, 22363548 and 22363547),
24 cell density and viability were measured as described above. Single cell RNA-Seq: 37,000 cells
25 (range: 15,000 ~ 40,000) were loaded into one well of 10X Genomics droplet-based scRNA-
26 Seq system and libraries were constructed by following the manufacturer’s protocol
27 “Chromium Next GEM Single Cell 3’ Reagent Kits with Feature Barcoding technology for Cell
28 Surface Protein, v3.0 or v3.1”. The libraries were sequenced for 546 million paired-end
29 fragments on average for cDNA and 96 million fragments for Hashtags using either Illumina
30 NextSeq 500 or NovaSeq 6000. The number of recovered cells was 12,436 on average (ranging
31 $5,208 \sim 44,126$)(STable 10). Variations on the main protocol: 89 of 172 samples were treated
32 using the procedure described above (“protocol 4”). 28 Samples were treated using “protocol

1 1" with the following specificities. After dissociating biopsies into cell suspensions, EC cell
2 fractions were sorted by FACS (BD Biosciences, FACSAria III Cell Sorter) to enrich living EC and
3 intraepithelial lymphocytes (IEL) using anti-human CD326 (Biolegend, 324226), CD45
4 (Biolegend, 304037), CD19 (Biolegend, 363034) and CD11b antibodies (Biolegend, 301348)
5 along with Zombie Green Fixable Viability Dye (Biolegend, 423112). In parallel, LP cell fractions
6 were sorted for living lymphocytes (LP-LC) and myeloid cells (LP-MC) by staining with anti-
7 human CD326, CD45 (Biolegend, 304032) and CD11b antibodies and Zombie Green Fixable
8 Viability Dye. The 12 fractions of sorted cells (EC, IEC, LP-LC and LP-MC for 3 locations) were
9 labeled using distinct TotalSeq-A anti-human Hashtag antibodies (Biolegend) and all cell
10 fractions loaded together on a single well of 10X Genomics Chromium system. 36 samples
11 were treated using "protocol 2" with the following specificities: living cells from EC and LP
12 fractions of cells were enriched using EasySep Dead Cell Removal Annexin V kit (Stemcell
13 technologies, 17899). 19 samples were treated using "protocol 3", with following
14 specificities: living cells from EC and LP fractions of cells were enriched using FACS by staining
15 cells with Zombie Green Fixable Viability Dye. General precautions: Samples were
16 manipulated on ice unless described and using low retention filter tips (e.g., RAININ,
17 30389213). Cell strainers were dipped in FBS before use. Samples retained on a cell strainer
18 were transferred by flipping the cell strainer on a collection tube and flushing it with a buffer.

19 **Preprocessing of scRNA-Seq data.** Raw sequencing data were preprocessed with the
20 Cellranger software version 7.1.0 with standard parameters and GRCh38 (Ensembl release
21 103) human genome build as reference. Processed counts were further analyzed in R (version
22 4.3.1) within the Seurat tools ecosystem (Seurat version 4.1.3 [Hao *et al.*, 2021]). For each
23 sample, mRNA read counts and hashtag barcode read counts were loaded to R and quality-
24 checked. We excluded (i) hashtag barcodes with < 300 reads per individual, (ii) cells with \geq
25 50% mitochondrial reads, (iii) cells with < 200 different genes expressed, (iv) cells with < 5
26 hashtag barcode reads. Demultiplexing of cells was done using two different algorithms
27 implemented in Seurat: HTODemux [Stoeckius *et al.*, 2018] (positive.quantile 0.999,
28 clusterization function - kmeans) and MULTIseqDemux [McGinnis *et al.*, 2019] with
29 automated threshold finding. Cells identified as singlets of the same tissue type by the two
30 methods were kept for further analysis. To meet the RAM usage requirements, variable
31 features selection was done in five sample batches with the "mean.var.plot" algorithm (3,000
32 features per batch). We retained the intersection between the five batches. We then

1 integrated the sample batches in the space defined by the first 50 principal components using
2 Harmony [Korsunsky *et al.*, 2019]. The UMAP plots shown throughout the manuscript (f.i. Fig.
3 2D and 2E) are in this coordinate system. Yet, to better differentiate cell types and improve
4 the clustering, we further split the data in two stages. We first used Hashtag information to
5 separate cells by anatomical location (IL, TC, RE). Within each anatomical location we
6 repeated the variable feature selection and integration process. In each of these three sub-
7 datasets, we identified cell clusters with the Louvain algorithm. Based on marker gene
8 expression, we assigned clusters to three groups: immune (expressing *PTPRC*), epithelial
9 (expressing *EPCAM*), and endothelial plus other cells (expressing *VWF*, *PECAM1*, *CDH5* or not
10 included in previous groups). Within each one of these nine sub-groups, we again repeated
11 variable features selection, integration and clustering (Louvain clustering algorithm with
12 resolution parameter 1.5). This yielded a total of 276 clusters across the nine data sets (SFig.
13 5).

14 **Constructing a hierarchical tree of cell clusters.** We computed, for each of the 276 location-
15 and cell-type specific cell clusters (obtained as described above), the mean coordinate vector
16 in the space of the first 50 Harmony coordinates. Then we computed the Euclidean distance
17 between these vectors followed by hierarchical clustering (function `hclust`, stats R package,
18 “complete” agglomeration method). The final dendrogram was constructed with the
19 `dendextend` [Galili, 2015] R package.

20 **Cis-eQTL analysis.** We performed eQTL analysis for each leaf and node in the hierarchical
21 tree, provided that the median cells per patient was ≥ 5 and that number of patients with
22 cells in the leaf/node was ≥ 30 . This left 401 leaves/nodes for eQTL analysis. Within each
23 analyzed leaf or node, all cells were treated as pseudo-bulk, i.e., as if all reads were derived
24 from one mega-cell. Resulting gene expression data were normalized using DESeq2,
25 residualized for age, sex and five genotype PCs, and corrected for hidden confounders utilizing
26 the probabilistic estimation of expression residuals (PEER) algorithm [Stegle *et al.*, 2010].
27 Association between gene expression and alternate allele dosage was conducted for each SNP
28 in a 2Mb-window centered on the gene’s transcription start site using QTLtools [Delaneau *et al.*,
29 2017]. Nominal *p*-values were corrected for the realization of multiple tests in this *cis*-
30 window by permutation, yielding a window-adjusted *p*-value for one lead SNP for every gene
31 x leaf/node combination. Window-adjusted lead SNP *p*-values for all genes in a leaf/node
32 were jointly used to compute a *q*-value using Storey & Tibshirani [2003].

1 **Agglomerating *cis*-eQTL in gene-specific and across-genes *cis*-acting regulatory modules**
2 **(RM).** The construction of *cis*-acting regulatory modules (RM) was done in a similar way as
3 for the circulating immune cell populations, across all 276 leaves and 275 nodes of the
4 hierarchical tree. We first build gene-specific and then across-gene modules. For gene-
5 specific modules, we computed θ [Momozawa *et al.*, 2018] between EAP obtained, for that
6 gene, in the different nodes/leaves. θ was computed in the 2Mb *cis*-window centered on the
7 gene's transcription start site (TSS) (the window used for *cis*-eQTL analysis). For across-gene
8 modules, we additionally computed θ between EAP of different genes, provided that their
9 2Mb *cis*-windows overlapped. θ was then computed for the union between the two 2Mb *cis*-
10 windows. For both gene-specific and across-gene windows, we only considered EAP pairs for
11 which at least one corresponded to a significant eQTL (within leaf/node FDR ≤ 0.05). We only
12 considered SNPs with eQTL nominal p -value ≤ 0.05 for at least one of the two EAP. EAP (from
13 the same or different genes) were merged in the same module if $|\theta| \geq 0.6$, and (in the case
14 one of the EAP pairs did not correspond to a significant eQTL) a p -value of the eQTL corrected
15 for the multiple SNPs tested in the window (by permutation, see above) ≤ 0.012 , as this
16 yielded mergers with FDR ≤ 0.05 (see DAP-EAP part, hereafter). To be part of a module, an
17 EAP had to satisfy these criteria with at least one significant member of the module. Once a
18 module was assembled (all member EAP determined), θ was computed between non-
19 significant members of the module to evaluate the tightness of the module (ideally one hopes
20 for $|\theta| \geq 0.6$ between all members; observed: "Proportion of links" in STable 13 and STable
21 14). Links between pairs of EAP within a module were given a sign (positive or negative)
22 depending of the value of θ . Constituent EAP were given a positive sign if their θ with the
23 module's representative EAP (the one with the most significant eQTL) was positive, a negative
24 sign otherwise. For modules that comprised more than one EAP, we computed a consensus
25 EAP (2-4 Mb window) by "meta-analysis". P -values for all SNPs in the window were converted
26 to z-scores, z-scores (for a given SNP) squared and summed over all members of the module.
27 The resulting sum was converted back to a p -value assuming that it had a chi-squared
28 distribution with numbers of degrees of freedom equal to the number of EAP in the module.
29 The EAP of all constituent eQTL were confronted to the consensus EAP in the full window. An
30 EAP was only maintained in the module if its $|\theta|$ -value with the consensus was ≥ 0.6 .
31 Otherwise, it was ejected from the module. Ejected EAP were confronted to each other and
32 given the possibility to assemble in new "sub-modules".

1 **Cell type annotation and cell type to hierarchical tree map.** Cell type annotation was largely
2 done by visually inspection of the expression profiles of 49 cell type-specific gene signatures
3 obtained from the literature [Smillie *et al.*, 2019; Franzen *et al.*, 2019; Burclaff *et al.*, 2022;
4 Ishikawa *et al.*, 2022; Hickey *et al.*, 2023; Kong *et al.*, 2023; Krzak *et al.*, 2023] using the Seurat
5 AddModuleScore function [Tirosh *et al.*, 2016], and the Azimuth human PBMC reference
6 mapping program for immune cells [Hao *et al.*, 2021], on our global UMAP (i.e., all 293,801
7 QC-ed cells) (Fig. 2D). In essence, the distribution of a cell type-specific gene-signature on the
8 UMAP was confronted with the distribution of the cells from each node/leaf of our
9 hierarchical tree, looking for best matches. A given cell-type was assigned to the best
10 matching node (and hence all descendent nodes/leaves). We further distinguished location-
11 specific (i.e., ileum, colon and rectum) nodes and leaves within cell type-specific sections of
12 the tree. The workflow and outcome of this analysis are shown in SFig. 8 and Stable 11.

13 **Assigning regulatory modules to intestinal cell types.** Regulatory modules encompass one
14 or more EAP that can be active in one or more nodes/leaves of the hierarchical tree. If all
15 nodes/leaves in which a module is active belong to the same cell type (see previous section),
16 the module was assigned to that cell type (and possibly anatomical location within cell type).
17 If nodes/leaves belonging to a module correspond to multiple cell types, the module was
18 assigned to one of 29 supergroups, listed in STable 11&17. As an example, if a module was
19 active in CD4 and CD8, it was assigned to the T lymphocyte supergroup.

20 **Exploring the distribution of the number of nodes/leaves in which regulatory modules are**
21 **active.** As for blood, each module is characterized by a vector of 0's and 1's informing us
22 about the nodes/leaves in which the module is active. In the case of the intestinal scRNA-Seq
23 data, the length of the vector is 155 leaves + 246 nodes = 401 elements. The length of the
24 vector is less than the sum of the total number of leaves and nodes in the module, because
25 some nodes/leaves didn't have any active module in them. The sum of 1's in a module vector,
26 i.e., the total number of leaves/nodes in which the module is active, is what we are looking at
27 in Fig. 3C. More specifically, we are looking at the distribution of this sum across all modules.
28 Conversely, the activity of a leaf/node can be summarized by a vector of 3,345 (gene-specific
29 modules) or 3,081 (across-gene modules) 0's and 1's, indicating which module is active in the
30 corresponding leaf/node. To verify whether the observed distribution differs from the
31 expected one, assuming that the activity of a module in a given leaf/node is independent of
32 its activity in other leaves/nodes, we assigned the 0's and 1's of a given leaf/node randomly

1 to the modules, i.e., we randomly permuted module id within leaf/node. We then summed
2 the number of 1's across the modules and examined the distribution of this sum across
3 modules (gray bars in Fig. 3C). We know that the activities of a module in adjacent
4 nodes/leaves in the tree are not independent, as these have cells in common. To properly
5 evaluate the statistical significance of the apparent “overdispersion” of module activity (too
6 many modules either active in few nodes/leaves, or in many nodes/leaves), we restricted to
7 the analysis to “parent” nodes of the 49 distinct cell types, selected such that no cell could be
8 part of more than one such cell type (i.e., none of the selected nodes is ancestor of any other
9 one). We quantified the dispersion for the real data, as the variance of the sum of active
10 nodes across modules. We then performed “permutations”, in the sense that – for a given
11 node – the activity states (1's and 0's) were permuted between modules. This was repeated
12 for all nodes, and the dispersion of that permutation computed as the variance of the sum of
13 “active” nodes across modules. The statistical significance of the real dispersion was then
14 defined as the proportion of permutations that yielded as large or larger variance than the
15 real data.

16 **3D plots of *cis*-eQTL activity.** We developed an application to visualize the activity of an eQTL
17 of interest on a 3D UMAP plot. Briefly, for each cell in the dataset, we identified the 100
18 nearest neighbors in the space defined by the 50 first expression principal components using
19 the Annoy algorithm [<https://github.com/spotify/annoy>] implemented in the Seurat
20 Findneighbors function. We eliminated cell-centered neighborhoods encompassing cells
21 from only one individual, less than five cells with non-null expression for the e-gene of
22 interest, and MAF < 0.05 for the eQTL's top SNP amongst the individuals with cells in the
23 neighborhood. We then performed eQTL analysis in the remaining neighborhoods, one at a
24 time, using a mixed model [Bates *et al.*, 2015; Kuznetsova *et al.*, 2017] including allele dosage
25 (for the eQTL's top SNP) as fixed regression, and individual as random effect. For each
26 neighborhood we then multiplied $-\log(p\text{-value})$ of the eQTL effect by the sign of the regression
27 coefficient (β), assigned it to the cell defining the neighborhood, and plotted it as the third, z
28 dimension of a 3D plot, at the x-y coordinate position corresponding to the position of the
29 reference cell in 2D UMAP space.

30

31 ***Merging blood and intestinal cis-eQTL modules reveals eQTLs that are specific for gut-***
32 ***resident immune cells***

1 **Module construction.** Constructing modules integrating blood and intestinal data followed
2 the same procedure as for the blood- and gut-specific modules. Requirements for an EAP to
3 join a module were the same as before, i.e., $|\theta| \geq 0.6$ for both blood and gut EAP, $p_\theta \leq 0.05$
4 for both blood and gut, $p_{eQTL,window\ adj} \leq 0.12$ for blood and ≤ 0.012 for gut. These
5 thresholds ensured an $FDR \leq 0.05$ in the corresponding DAP-EAP confrontations (see
6 hereafter).

7 **Test of independence of cell type annotation in blood and gut.** Modules were assigned to
8 cell types separately for blood cell type populations (obvious) and intestinal cell type
9 populations (using the same approach as for the intestinal modules). One expects a certain
10 degree of coherence with regards to cell type assignment in both datasets. As an example,
11 modules that are assigned to lymphocytes in blood are expected to be assigned to the
12 lymphoid compartment in the intestine as well. We verified this concordance by performing
13 an empirical test of independence. Cell types were groups in a limited number of
14 “supergroups” (Blood: lymphoid, myeloid other than granulocytes, granulocytes, multiple cell
15 types, undetected; Gut: lymphoid, myeloid, enterocyte precursor, mature enterocyte,
16 stromal, multiple cell types, undetected; see also Fig. 4B). We first performed a test of
17 independence within the group of 2,170 modules that were assigned to a supergroup in both
18 data sets. We determined the proportion of modules assigned to each supergroup separately
19 for blood (p_i^{Blood}) and gut (p_j^{Gut}). The observed number of modules assigned to supergroup
20 i in blood and j in gut was then compared to the expected number computed as $2,170$
21 $\times p_i^{Blood} \times p_j^{Gut}$. The probability to obtain an as large or larger deviation between expected
22 and observed numbers by chance was determined from 1,000 replicates of 2,170 samplings
23 with replacement with a probability of success of $p_i^{Blood} \times p_j^{Gut}$. Secondly, within the group
24 of 4,579 modules that were active in gut alone, we determined the proportion that were
25 assigned to each one of the gut supergroups (p_j^{Gut}) as well as the proportion that were not
26 active in blood (p_{ND}^{Blood}). The observed number of modules assigned to supergroup j in gut
27 yet undetected in blood was then compared to the expected number computed as $4,579$
28 $\times p_{ND}^{Blood} \times p_j^{Gut}$. The probability to obtain an as large or larger deviation between expected
29 and observed numbers by chance was determined from 1,000 replicates of 4,579 samplings
30 with replacement with a probability of success of $p_{ND}^{Blood} \times p_j^{Gut}$. Finally, within the group of
31 22,336 modules that were active in blood alone, we determined the proportion that were

1 assigned to each one of the gut supergroups (p_i^{Blood}) as well as the proportion that were not
2 detected in gut (p_{ND}^{Gut}). The observed number of modules assigned to supergroup i in blood
3 yet undetected in gut was then compared to the expected number computed as $22,336$
4 $\times p_i^{Blood} \times p_{ND}^{Gut}$. The probability to obtain an as large or larger deviation between expected
5 and observed numbers by chance was determined from 1,000 replicates of 22,336 samplings
6 with replacement with a probability of success of $p_i^{Blood} \times p_{ND}^{Gut}$.

7

8 **Identifying new cis-eQTL driving inherited predisposition to IBD**

9 **Comparing EAP and DAP using theta.** We performed a colocalization analysis of our EAP with
10 IBD, CD and UC risk loci coming from de Lange *et al.* [2017]. We lifted their data over from
11 GRCh37 to GRCh38 and defined disease association patterns (DAP) in genomic locations
12 where a risk locus was described in at least one of the diseases and where at least one variant
13 had a p -value less or equal to 10^{-5} . We established the limits of the DAPs manually to surround
14 the peaks. In total, we tested 455 DAP corresponding to 206 risk loci (157 for CD, 173 for IBD
15 and 125 for UC). Some DAP were subdivided into two or three parts. We evaluated the
16 similarity between DAP and EAP using θ following Momozawa *et al.* [2018], for all EAP for
17 which the top eQTL SNP was within the boundaries of the analyzed disease interval. θ was
18 computed for all variants located within the limits of the disease interval, provided that their
19 nominal association p -value ≤ 0.05 either in the EAP, DAP or both. To determine the
20 statistical significance of θ (i.e., p_θ), we performed up to (adaptive) 10,000 permutations
21 (without replacement) of gene expression levels before recomputing θ . We defined p_θ as the
22 proportion of permutations where the obtained $|\theta|$ is greater or equal to the observed.

23 To further define appropriate thresholds to declare a DAP-EAP match of interest, we repeated
24 the full, genome-wide cis-eQTL analysis, both in blood and gut (i.e., in the 27 cell types and
25 551 leaves/nodes), after randomly disconnecting (i.e., permuting) the genotype (all variants)
26 and expression (all genes) vectors. Genotype and expression vectors were maintained
27 unaltered (hence LD structure on the one hand, and correlation structure between gene
28 expression on the other hand, were conserved). We then repeated the colocalization exercise
29 between all 455 DAPs, and the overlapping EAP obtained with the permuted data exactly as
30 we did with the real data. Assume that a DAP matches a real EAP with $|\theta| = x \geq 0.6$, $p_\theta =$
31 y , and $p_{eQTL,window adj} = z$, we would determine how many matches satisfying $|\theta| \geq x$, $p_\theta \leq$

1 y , and $p_{eQTL,window\ adj} \leq z$, were obtained with the real data ($= N_R$) and how many with the
2 permuted data ($= N_P$). The FDR of the corresponding DAP-EAP match was then computed
3 as $\frac{N_P}{N_R}$. We defined two FDR thresholds of significance: Tier 1 ($FDR \leq 0.05$) and Tier 2
4 ($0.05 < FDR \leq 0.10$).

5 **Differential expression analysis between active CD patients and controls.** We collected
6 blood from 55 active CD patients and performed RNA-Seq on the 27 fractionated circulating
7 immune cell populations. Differential expression analysis between controls and patients was
8 performed by cell type using the DESeq2 R package [Love *et al.*, 2014], with the apeglm
9 method for effect size shrinkage [Zhu *et al.*, 2019]. Genes with a fold change above 1.5 and
10 an adjusted p-value below 0.05 were considered differentially expressed (STable 26).

11 **Comparing the number of DAP-EAP matches with the CEDAR2 cell-type specific information
12 from ≤ 200 individuals versus the eQTLGen PBMC information from 35 K individuals.**

13 Summary statistics from eQTLGen, a meta-analysis of *cis*-eQTL results from 37 studies of
14 blood and PBMC samples totaling 35K individuals, were downloaded (Vösa *et al.*, 2021). We
15 lifted their data over from GRCh37 to GRCh38. When arithmetic underflow was observed for
16 the p -values, the \log_{10} p -values were predicted from the z-scores using a local polynomial
17 regression. We compared their 871 EAP (significant or not) with the 455 DAPs if the top
18 variants were located within the disease interval. However, it was not possible to recompute
19 the missing part of the EAP nor to compute a p -value for theta. Colocalized EAP correspond
20 to EAP that have a $|\theta| \geq 0.6$ with a DAP (hence more permissive than the analysis of the
21 CEDAR2 dataset).

22

23 **Additional references**

24 Bates D, Mächler M, Bolker B, Walker S. "Fitting Linear Mixed-Effects Models Using lme4." *Journal of Statistical
25 Software* **67**: 1–48 (2015). [doi:10.18637/jss.v067.i01](https://doi.org/10.18637/jss.v067.i01).

26 Galili T. dendextend: an R package for visualizing, adjusting and comparing trees of hierarchical clustering.
27 *Bioinformatics* **31**:3718-3720 (2015). <https://doi.org/10.1093/bioinformatics/btv428>.

28 Hao Y, Hao S, Andersen-Nissen E, Mauck III WM, Zheng S, Butler A, Lee MJ, Wilk AJ, Darby C, Zager M, Hoffman
29 P, Stoeckius M, Papalexi E, Mimitou EP, Jain J, Srivastava A, Stuart T, Fleming LM, Yeung B, Rogers AJ, McElrath
30 JM, Blish CA, Gottardo R, Smibert P, Satija R. Integrated analysis of multimodal single-cell data. *Cell* **184**: 3573-
31 3587 (2021). <https://doi.org/10.1016/j.cell.2021.04.048>.

32 Korsunsky I, Millard N, Fan J, Slowikowski K, Zhang F, Wei K, Baglaenko Y, Brenner M, Loh P-r, Raychaudhuri S.
33 Fast, sensitive and accurate integration of single-cell data with Harmony. *Nat Methods* **16**: 1289–1296 (2019).
34 <https://doi.org/10.1038/s41592-019-0619-0>

35 Kuznetsova A, Brockhoff PB, Christensen RHB. "lmerTest Package: Tests in Linear Mixed Effects Models."
36 *Journal of Statistical Software* **82**: 1–26 (2017). [doi:10.18637/jss.v082.i13](https://doi.org/10.18637/jss.v082.i13).

- 1 McGinnis CS, Patterson DM, Winkler J. *et al.* MULTI-seq: sample multiplexing for single-cell RNA sequencing
2 using lipid-tagged indices. *Nat Methods* **16**: 619–626 (2019). <https://doi.org/10.1038/s41592-019-0433-8>
- 3 Stoeckius M, Zheng S, Houck-Loomis B. *et al.* Cell Hashing with barcoded antibodies enables multiplexing and
4 doublet detection for single cell genomics. *Genome Biol* **19**: 224 (2018). [https://doi.org/10.1186/s13059-018-](https://doi.org/10.1186/s13059-018-1603-1)
5 [1603-1](https://doi.org/10.1186/s13059-018-1603-1)
- 6 Tirosh I, Izar B, Prakadan SM, Wadsworth MH 2nd, Treacy D, Trombetta JJ, Rotem A, Rodman C, Lian C, Murphy
7 G, Fallahi-Sichani M, Dutton-Regester K, Lin JR, Cohen O, Shah P, Lu D, Genshaft AS, Hughes TK, Ziegler CG, Kazer
8 SW, Gaillard A, Kolb KE, Villani AC, Johannessen CM, Andreev AY, Van Allen EM, Bertagnolli M, Sorger PK, Sullivan
9 RJ, Flaherty KT, Frederick DT, Jané-Valbuena J, Yoon CH, Rozenblatt-Rosen O, Shalek AK, Regev A, Garraway LA.
10 Dissecting the multicellular ecosystem of metastatic melanoma by single-cell RNA-seq. *Science* **352**:189-196
11 (2016). doi: 10.1126/science.aad0501.

12

13 **Acknowledgments**

14 This project was conducted with funding from the SYSCID H2020 grant (ref. 733100, the
15 MyQuant (ref. 30770923) and BRIDGE (O.0006.22 – RG3124) projects from the Excellence of
16 Science (EOS) program (FNRS, Fédération Wallonie-Bruxelles and FWO, Flemish Community),
17 the CLIMAX (WELBIO-CR-2022 A) project from WELBIO (Walloon Region), the RHEAQT
18 (T.0096.19) and IBD-GI-Seq (T.0190.19) projects from the FNRS (Fédération Wallonie-
19 Bruxelles), the ARC RHEACT WITH HSPC project from the University of Liège. Computational
20 resources have been provided by the Consortium des Équipements de Calcul Intensif (CÉCI),
21 funded by the Fonds de la Recherche Scientifique de Belgique (F.R.S.-FNRS) under Grant No.
22 2.5020.11 and by the Walloon Region. We thank Sandra Ormenese, Celine Vanwinge and the
23 GIGA-Flow cytometry core facility for their support, as well as Naima Ahariz, Azeddine Bentaib
24 and the other members of the GIGA genomics platform. Souad Rahmouni is a senior research
25 associate of the FRS-FNRS. We are grateful to Yurii Aulchenko for many stimulating
26 discussions.

27

28 **Members of the SYSCID Consortium:** Konrad Aden, Vibeke Andersen, Diana Avalos, Aggelos
29 Banos, George Bertias, Marc Beyer, Johanna I Blase, Dimitrios Boumpas, Emmanouil T
30 Dermitzakis, Axel Finckh, Andre Franke, Gilles Gasparoni, Michel Georges, Wei Gu, Robert
31 Häslér, Mohamad Jawhara, Amy Kenyon, Christina Kratsch, Roland Krause, Gordan Lauc, Paul
32 A Lyons, Massimo Mangino, Neha Mishra, Gioacchino Natoli, Marek Ostaszewski, Silja H
33 Overgaard, Marija Pezer, Jeroen Raes, Souad Rahmouni, Benedikt Reiz, Elisa Rosati, Philip
34 Rosenstiel, Despina Sanoudou, Venkata Satagopam, Reinhard Schneider, Jonas Schulte-
35 Schrepping, Joachim L Schultze, Prodromos Sidiropoulos, Kenneth GC Smith, Signe B
36 Sørensen, Timothy Spector, Doris Vandeputte, Sara Vieira-Silva, Aleksandar Vojta, Jörn

- 1 Walter, Stefanie Warnat-Herresthal, and Vlatka Zoldoš. **Members of the BRIDGE Consortium:**
- 2 Inna Afonina, Rudi Beyaert, Laure Dumoutier, Denis Franchimont, Michel Georges, Claude
- 3 Libert, Claire Liefferinckx, Natalia Ferreras Moreno, Souad Rahmouni, Ramnik Xavier.
- 4
- 5